Bioactive Materials 52 (2025) 228–243

Contents lists available at ScienceDirect

Bioactive Materials

journal homepage: www.keaipublishing.com/en/journals/bioactive-materials

Biomimetic extracellular vesicles derived from chimeric antigen receptor monocytes to treat glioblastoma: An efficient and safe intranasal drug delivery nanoplatform

Qihong Cheng [a,1], Minjie Wang [a,1], Zijie Zhou [a,1], Huitang Xia [b,c,d,*], Shaojie Yu [a], Jianglin Zheng [a], Kai Zhu [a], Xudong Li [a], Xuan Wang [a], Tao Xin [b,d,e,**], Xiaobing Jiang [a,***], Junjun Li [a,****]

[a] Department of Neurosurgery, The Union Hospital of Tongji Medical College, Huazhong University of Science and Technology, Wuhan, 430022, PR China
[b] Department of Neurosurgery, The First Affiliated Hospital of Shandong First Medical University & Shandong Provincial Qianfoshan Hospital, Jinan, 250014, PR China
[c] Jinan Clinical Research Center for Tissue Engineering Skin Regeneration and Wound Repair, Jinan, Shandong, 250014, PR China
[d] Shandong Engineering Research, Center of Precision Diagnosis and Treatment Technology for Neuro-oncology, Jinan, 250014, PR China
[e] Laboratory of Basic and Translational Neuromedicine, The First Affiliated Hospital of Shandong First Medical University, Jinan, 250014, PR China

ARTICLE INFO

Keywords:
Extracellular vesicle mimetics
Chimeric antigen receptors
Membrane extrusion
Intranasal administration
Glioblastoma

ABSTRACT

Background: Extracellular vesicles (EVs) have emerged as a promising pharmacotherapeutic modality for glioblastoma (GBM) drug delivery. However, the clinical translation of EVs remains restricted due to their low yield and demanding extraction steps. Therefore, extracellular vesicle mimetics (EVMs), as alternatives to EVs, have received much attention.

Results: Herein, inspired by the inherent GBM tropism of monocytes and the editable target recognition ability of chimeric antigen receptors (CARs), we present the synthesis and systemic evaluation of a doxorubicin (DOX)-loaded nanoplatform (termed CAR-EVMs@DOX) generated by loading DOX into EVMs derived from CAR-modified monocytes (CAR-EVMs) via a modified extrusion method. Due to insufficient GBM drug delivery efficacy and great systemic toxicity caused by the resistance of the blood−brain barrier (BBB), CAR-EVMs@DOX can be administered intranasally to bypass the BBB, resulting in dramatic GBM-targeted migration and accumulation in the GBM site. Moreover, compared with intravenous administration, intranasal delivery of CAR-EVMs@DOX increases tumor inhibition efficacy while protecting against DOX-induced cardiotoxicity.

Conclusions: The findings of our study demonstrate that the intranasal administration of the facile and well-designed nanoplatform CAR-EVMs@DOX is an advanced drug delivery tactic for GBM therapy, with the potential for future clinical translation.

1. Introduction

Glioblastoma (GBM), as the most prevalent malignant neoplasm of the central nervous system (CNS), has a bleak prognosis, with a five-year relative survival rate of approximately 5 % [1]. Conventional GBM therapy mainly includes surgical resection and postoperative

Peer review under the responsibility of editorial board of Bioactive Materials.

* Corresponding authors. Department of Neurosurgery, The First Affiliated Hospital of Shandong First Medical University & Shandong Provincial Qianfoshan Hospital, Jinan, 250014, PR China.

** Corresponding author. Department of Neurosurgery, The First Affiliated Hospital of Shandong First Medical University & Shandong Provincial Qianfoshan Hospital, Jinan, 250014, PR China.

*** Corresponding author.

**** Corresponding author.

E-mail addresses: m202275948@hust.edu.cn (Q. Cheng), 2023XH0116@hust.edu.com (M. Wang), zijie.zhou2@astrazeneca.com (Z. Zhou), 3083@sdhospital.com.cn (H. Xia), d202382102@hust.edu.cn (S. Yu), 2020508093@hust.edu.cn (J. Zheng), kaizhu@hust.edu.cn (K. Zhu), d202381951@hust.edu.cn (X. Li), 2012xh0864@hust.edu.cn (X. Wang), xintao@sdfmu.edu.cn (T. Xin), 2004xh0835@hust.edu.cn (X. Jiang), 2020xh0063@hust.edu.cn (J. Li).

[1] Qihong Cheng, Minjie Wang and Zijie Zhou contributed equally.

https://doi.org/10.1016/j.bioactmat.2025.05.032
Received 23 February 2025; Received in revised form 17 May 2025; Accepted 28 May 2025

chemoradiotherapy. Unfortunately, due to the highly invasive nature of GBM and insufficient tumor drug delivery that is mainly affected by the presence of the blood−brain barrier (BBB), GBM patients have a grim median overall survival (OS) of 15–18 months [2,3]. Furthermore, chemotherapeutic agents lacking efficiency for drug delivery to the brain and targeting abilities are accompanied by substantial systemic toxicity [4]. Thus, these obstacles remain great challenges in the efficient accumulation of chemotherapeutic agents in the tumor site.

Extracellular vesicles (EVs) are cell-secreted phospholipid bilayer-enclosed structures that serve as intercellular messengers to transport intracellular cargos to recipient cells [5–7]. EVs can be divided into three subtypes according to particle size: exosomes (30–150 nm), microvesicles (50–1000 nm) and apoptotic bodies (50–2000 nm). Due to their superiority in terms of stability in circulation, biocompatibility, intrinsic tropism, inherent targeting ability and capability to cross biological barriers, the application of EVs as drug delivery platforms has emerged as a novel pharmacotherapeutic treatment modality for GBM [8,9]. Despite these advantages, the applications of EVs are limited due to the low yields and demanding extraction steps required to obtain naturally secreted EVs [10].

Recently, extracellular vesicle mimetics (EVMs), as alternatives to EVs, have received much attention [11–13]. EVMs can be manufactured in high yield through mechanical extrusion and possess lipids and proteins similar to those of the derived cells. In addition to their superior yield, compared to natural EVs, EVMs have preferable stability and targeting abilities [14] and thus have been applied to treat various types of tumors [15,16]. Additional research on the applications of EVs/EVMs for tumor therapy has focused on how to increase the tumor-targeting ability while minimizing the uptake by other organs to the greatest extent. Various attempts have been made to achieve these aims, including exploring different source cells with intrinsic tumor tropism, amending vesicles with molecules or materials that have a specific targeting capacity, and seeking different modes of administration [17–19].

Monocytes, a main type of blood cell, have been shown to be capable of invoking GBM tropism and infiltrate in response to the chemokines secreted by GBM cells [20]. Monocyte-derived macrophages and microglia together constitute tumor-associated macrophages (TAMs), which account for nearly 30 % of cells in the GBM tumor microenvironment (TME) [21]. It is worth noting that recent studies have demonstrated that most TAMs originate from circulating precursor cells, although some are derived from tissue-resident microglia [20,22]. These features may allow monocytes and their EVMs to become advanced carriers for GBM drug delivery.

Chimeric antigen receptors (CARs) are human-modified receptors that can recognize a target antigen without major histocompatibility complex presentation [23]. CAR recognition capacity is mainly based on single-chain variable fragments (scFvs) derived from monoclonal antibodies [24]. Compared to other types of engineered antigen-binding domains, CAR sequences are entirely human, induce lower immunogenicity and can be engineered to recognize virtually all tumor-associated antigens [25,26]. To date, cell therapy based on CARs has exhibited tropism with various types of tumors [27–30]. Epidermal growth factor receptor variant III (EGFRvIII) is an ideal GBM-associated target in CAR-based therapy, as it is overexpressed in nearly 30 % of GBM patients [31]. Herein, to better elevate the tumor-targeting ability of EVMs, we employed membrane-bound EGFRvIII-specific CARs to endow the EVMs with the capability to selectively accumulate in EGFRvIII-overexpressing GBM.

Notably, intranasal administration is a noninvasive nose-to-brain drug delivery approach that not only bypasses the BBB but also reduces drug-related systemic toxicity [32]. As an ideal route to deliver drugs to the CNS, the trigeminal and olfactory nerve pathways can be utilized to ensure highly efficient accumulation of the therapeutic drug in the brain [33].

Taking these factors into consideration, we developed an intranasal drug delivery nanoplatform (CAR-EVMs@DOX) based on EVMs derived from CAR-modified monocytes to deliver doxorubicin (DOX) for the treatment of GBM. DOX was encapsulated by CAR-EVMs to facilitate GBM targeting. Compared to conventional intravenous administration, intranasal delivery of our nanoplatform produced superior therapeutic effects and reduced systemic cardiotoxicity (Fig. S1).

In summary, the engineered CAR-EVMs@DOX, when administered intranasally, is a neoteric nanomedicine for targeted GBM therapy with feasible potential for biomedical use and clinical translation in the future.

2. Materials and methods

2.1. Cell culture and animals

All the cell lines involved in this study were obtained from the National Infrastructure of Cell Line Resource. The U87MG cell line stably expressing EGFRvIII, U87MG cell Negative Control (U87NC) and a firefly luciferase (fluc) tag was obtained and amplified in our previous study [34]. The anti-EGFRvIII-CAR-THP-1 cell line was constructed via viral transfection and sorted with flow cytometry. Anti-EGFRvIII-CAR was encoded by a lentiviral vector and contained a humanized anti-EGFRvIII scFv, the hinge and transmembrane domains of CD8, the costimulatory domain of 4-1BB and the CD3ζ T-cell activation domain. U87MG cells and HOPC cells were incubated in DMEM. HUVECs, THP-1 cells and bEnd.3 cells were incubated in RPMI-1640 medium. Ten percent fetal bovine serum (FBS) and 1 % penicillin−streptomycin were added to the medium, and the cells were cultivated in a humid atmosphere with 5 % CO2 at 37 °C. In line with the NIH Animal Research and Care guidelines, the animal experimental protocol was established and approved by the Ethics Committee of Huazhong University of Science and Technology (No. 2022–3008). Six-week-old female BALB/c-nu nude mice were obtained from Hubei Biont Biotechnology Co., Ltd. (China).

2.2. Preparation and characterization of CAR-EVMs@DOX/EVMs@DOX

CAR-EVMs@DOX/EVMs@DOX was synthesized as described previously with some modifications [15]. Briefly, 1×10^6 CAR-THP-1/THP-1 cells were collected and mixed with DOX (400 μg mL-1) and then serially extruded through 10 μm, 1 μm, and 400 nm polycarbonate membranes (Whatman, UK) using an extruder (Avestin, Canada). The extruded product was then incubated for 4 h to enhance DOX loading. Next, the solution was filtered through a 0.22 μm filter followed by ultracentrifugation (110,000×*g*, 70 min) and washing with cold PBS to remove the dissociated DOX. The ultracentrifugation and washing steps were repeated twice, and the final CAR-EVMs@DOX was resuspended in PBS. Native CAR-EVs were isolated from the supernatant of CAR-THP-1 cells as described previously [4]. Briefly, after 1×10^6 CAR-THP-1 cells had been cultured for 72 h, the supernatant was collected and centrifuged at 1000×*g* for 10 min, 2000×*g* for 10 min and 10,000×*g* for 30 min, followed by filtration through a 0.22 μm filter to remove cell debris and large EVs. The filtered supernatant underwent ultracentrifugation (100,000×*g*, 70 min), and the product was washed with cold PBS. The ultracentrifugation and wash steps were repeated twice. Finally, CAR-EVs were resuspended in PBS. All of the above incubation and centrifugation procedures were carried out at 4 °C. The morphology of the EVs and EVMs was analyzed using a Hitachi HT7000 transmission electron microscope (Hitachi, Japan). The protein profile of CAR-EVMs@DOX and native CAR-EVs, including EV protein markers (CD9, CD63, TSG101) and some classic chemokine receptors expressed on THP-1 cells (CCR2, CXCR4, CSF1R), was analyzed via western blotting. The size distribution and yield of native EVs and EVMs presented in this manuscript were quantified by NTA using a ZetaVIEW S/N 17–310 (Particle Metrix, Germany). EVMs and EVs derived from 1×10^8 THP-1 were collected and analyzed by Western blot. The fluorescence colocalization of CAR-EVMs labeled with PKH67 and DOX was recorded with a confocal

microscope (PerkinElmer, USA), and the results were analyzed by ImageJ software. CAR expression on CAR-EVMs@DOX and CAR-EVs was assessed with FITC-conjugated Protein L (2 μg/10^7 particles; Acro Biosystems, China). In brief, the nanoagents or native EVs were incubated with FITC-conjugated Protein L for 2 h at 4 °C followed by washing steps with PBS. Then, the samples were analyzed using a NanoFCM N30E instrument (NanoFCM, UK). The results were analyzed with FlowJo V10 software (FlowJo, USA).

2.3. Measurement of DOX loading capacity and DOX loading efficiency

The amount of DOX loaded in the CAR-EVMs@DOX and EVMs@DOX was measured as the weight of DOX per number of particles. Briefly, 100 μl of CAR-EVMs@DOX solution was mixed with 100 μl of 0.5 % Triton X-100 and vortexed to release the DOX that had been loaded into the EVMs/CAR-EVMs. Then, the solution was incubated at 37 °C for 1 h, the absorbance was measured with a UV–visible spectrophotometer (Life-Real, China) at a wavelength of 480 nm, and the amount of DOX was calculated according to a preestablished DOX standard curve (Fig. S2a). The corresponding number of particles was determined using NTA. The encapsulation efficiency (EE) of DOX in CAR-EVMs@DOX and EVMs@DOX was determined as follows: $EE = M_{DOX\text{-}loaded}/M_{DOX\text{-}added}$. The loading efficiency (LE) of DOX in CAR-EVMs@DOX and EVMs@-DOX was determined as follows: $LE = M_{DOX\text{-}loaded}/M_{particle}$. $M_{DOX\text{-}loaded}$ is the amount of DOX loaded in the CAR-EVMs@DOX and EVMs@DOX calculated previously. $M_{particle}$ is the total masses of CAR-EVMs@DOX and EVMs@DOX synthesized previously. $M_{DOX\text{-}added}$ is the amount of DOX extruded and incubated with THP-1 mentioned above.

2.4. CCK8 assay

CCK8 Assay was performed by CCK8 kit (MCE, China) following the standard manual. Briefly, EVMs@DOX/CAR-EVMs@DOX (10^3 particles/cell), equal mess of doxorubicin hydrochloride (freeDOX, 2.3 × 10^{-3} ng/cell) or equal volume DMEM were incubated with U87NC and EGFRvIII-positive U87 cells respectively. After co-cultured for 8 h, cells were digested and resuspended. Then the above suspension was added into a 96-well plate (2000 cell/well) and cultured at 37 °C in 5 % CO_2 for 48 h. CCK8 was then diluted with serum-free DMEM and 100 μl 10 % CCK8 solution was added into the 96-well plate from which the culture medium was discarded. After incubation for 2 h in dark, the absorbance of the solution in each well at a wavelength of 450 nm was detected by Full wavelength microplate reader (Thermo Fisher, USA).

2.5. Clonal formation assay

Clonal formation assay evaluated the inhibition on the proliferation of glioblastoma cell lines. Briefly, U87NC and EGFRvIII-positive U87 cells were seeded in six-well plates, with 2000 cells per well. Subsequently, the two types of cells were added with CAR-EVMs@DOX/EVMs@DOX (10^3 particles/cell), equal mess of doxorubicin hydrochloride (free DOX, 2.3 × 10^{-3} ng/cell) or equal volume of DMEM for 8 h. Next, the culture medium was replaced with DMEM (with 10 % FBS and 1 % penicillin–streptomycin) and cultured at 37 °C in 5 % CO2 for 14 days. The cells in six-well plates were then washed twice with PBS and fixed in 4 % paraformaldehyde for 30 min. The fixed cells were stained with 0.1 % crystal violet solution for 1 h and then washed three times with PBS. The colored clones were photographed and counted.

2.6. Western blot

Western blot was used to detect the protein characteristics expressed by cells and EVMs. Briefly, the proteins of EVMs/CAR-EVMs and CAR-THP-1/THP-1 were extracted by PIPA lysis buffer (Beyotime, China), and the protein content was determined using BCA kit (Thermo Fisher, USA). The primary and secondary antibodies were used to indicate the bands of target proteins. Finally, enhanced chemiluminescence (ECL) solution (Epizyme Biotech, China) and protein imager (baygenebiotech, China) were used to visualize protein bands. Equal volumes of DMEM, EVMs@DOX/CAR-EVMs@DOX (10^3 particles/cell) or equal mess of doxorubicin hydrochloride (freeDOX, 2.3 × 10^{-3} ng/cell) were added into the mediums of U87NC and EGFRvIII-positive U87 cells and cultured for 8 h. Then the above eight groups were collected and subjected to Western blot according to the method described in this experiment. To extract protein of cardiac tissue, we cut the myocardium of the sacrificed mice, then add the lysis buffer and grinded it at a low temperature. The tissue homogenate after grinding was filtered and centrifuged. Then supernatant was used to measure the protein concentration and perform Western blot as described above. The primary and secondary antibodies used in this study are listed in Table S1. The protein bands were analyzed by ImageJ software.

2.7. Flow cytometry

Flow cytometry was used to detect the proportion of apoptotic cells. FITC-conjugated Annexin V was used to stain apoptotic cells. Briefly, equal volumes of DMEM, EVMs@DOX/CAR-EVMs@DOX (10^3 particles/cell) or equal mess of doxorubicin hydrochloride (freeDOX, 2.3 × 10^{-3} ng/cell) were added into the mediums of U87NC and EGFRvIII-positive U87 cells and the samples were harvested after 8 h of culture. After being washed twice with PBS, the harvested cells were resuspended in 1 × loading buffer at a concentration of 1 × 10^6 cells/ml. 100 μl of cell suspension was taken and 5 μl of FITC-conjugated Annexin V was added, and incubated at room temperature (RT) in the dark for 15 min. Subsequently, 400 μl of 1 × loading buffer was added. Cell fluorescence was then detected by flow cytometry (Becton, Dickinson and Company, USA). The results were analyzed with FlowJo V10 software (FlowJo, USA).

2.8. Fluorescent labeling of CAR-EVMs@DOX/EVMs@DOX

For in vitro cellular uptake studies, native EVs and EVMs were labeled with PKH67/PKH26 for tracing. In brief, EVs or EVMs were incubated with 5 μM PKH67 (MINI67, Sigma, USA) or PKH26 (MINI26, Sigma, USA) for 30 min at room temperature (RT) and diluted with cold PBS, followed by a washing step via ultracentrifugation (110,000×*g*, 70 min). For the in vivo distribution studies, native EVs and EVMs were labeled with the lipophilic carbocyanine dye DiIC18 (DiR) (Yeason, China) at a DiR concentration of 50 μg/mL. The other labeling and washing procedures were the same as those for PKH67/PKH26. The procedure by which EVMs@DOX and CAR-EVMs@DOX were labeled was the same as that described above.

2.9. Assessment of the tumor targeting ability and drug delivery properties of CAR-EVMs@DOX In vitro

First, to assess the tumor-targeting abilities of CAR-EVMs and EVMs, 0.5 × 10^5 cells (EGFRvIII-positive U87 cells, bEnd.3 cells, HUVEC cells or HOPC cells) were seeded on a 24-well culture plate and cultivated to attach. Then, filamentous actin (F-actin) was labeled with Alexa Fluor 488-conjugated phalloidin (Invitrogen, USA), and the cell nuclei were stained with DAPI. Next, the cells were incubated with PKH26-labeled EVMs or CAR-EVMs (10^3 particles/cell) for 2, 4 or 8 h. Thereafter, the cells were washed with PBS and fixed with 4 % paraformaldehyde for further detection via an UltraVIEW VoX Spinning Disk confocal microscope (PerkinElmer, USA). The fluorescence images were analyzed by ImageJ software.

In addition, the procedure by which the drug delivery properties of CAR-EVMs@DOX and EVMs@DOX were evaluated was similar to that of CAR-EVMs and EVMs, except that CAR-EVMs@DOX and EVMs@DOX were labeled with PKH67. To evaluate the BBB penetration ability of CAR-EVMs and EVMs, an in vitro BBB model with a Transwell chamber

was constructed according to a previous study [4]. Briefly, 0.5×10^5 EGFRvIII-positive U87 cells were seeded in the bottom chamber, and 1×10^5 bEnd.3 cells were seeded on precoated Matrigel (BD Biosciences, USA) in the upper chamber (pore size = 0.4 μm). The bEnd.3 layers with transepithelial electrical resistance (TEER) values higher than 300 Ω cm^2 were considered a qualified model for further evaluation. DAPI was applied to label the cell nuclei. PKH67-labeled EVMs@DOX and CAR-EVMs@DOX were added to the upper chamber (10^3 particles/cell) and incubated for 2, 4, or 8 h. Afterward, the cells in the upper and bottom chambers were washed with PBS and fixed with 4 % paraformaldehyde for detection via confocal microscopy.

2.10. Evaluation of the tumor targetability of CAR-EVMs@DOX In vivo

An orthotropic GBM mouse model was constructed in line with a previously described procedure [17]. In brief, 5×10^5 EGFRvIII-positive U87 cells expressing the luciferase gene were injected into the right striatum (2 mm lateral, 1 mm longitudinal and 3 mm deep) of 6-week--old female BALB/c-nu nude mice postanesthesia. Ten days later, the mice were treated with an intraperitoneal injection of D-luciferin (Yeason, China) 150 mg/kg followed by in vivo bioluminescence imaging using an in vivo spectrum imaging system (IVIS Spectrum, Caliper, America) to determine the success of tumor inoculation. The tumorigenic mice were randomly divided into six groups (I: intranasal delivery of free DiR (n = 3); II: intranasal delivery of EVMs@DOX (n = 3); III: intranasal delivery of CAR-EVMs@DOX (n = 3); IV: intravenous delivery of free DiR (n = 3); V: intravenous delivery of EVMs@DOX (n = 3) and VI: intravenous delivery of CAR-EVMs@DOX (n = 3)). Free DiR was administered at a dose of 1 mg/kg, and EVMs@DOX and CAR-EVMs@DOX were administered at a dose of 3×10^{10} particles dissolved in 20 μl of saline. EVMs@DOX and CAR-EVMs@DOX were labeled with DiR before intranasal or intravenous administration (tail vein injection). Then, the mice were transferred to cages and subjected to observation with the IVIS imaging system (IVIS Spectrum, Caliper) to monitor the migration of DiR fluorescence (excitation wavelength: 740 nm; emission wavelength: 780 nm) toward the tumor site at 4, 8, 16 and 24 h postadministration. After the last images were taken, the mice were sacrificed, and the brain and heart tissues were collected and subjected to ex vivo imaging to monitor DiR fluorescence. Next, for CAR-EVMs@DOX tracing, the brain tissue of the mice in the intranasal CAR-EVMs@DOX delivery group was immediately frozen at −80 °C, and 7 μm frozen sections were stained with DAPI followed by detection via confocal microscopy.

2.11. In vivo evaluation of Anti-GBM efficacy with orthotropic GBM models

To determine anti-GBM efficacy, the same orthotropic GBM model that was constructed and applied in the previous section was used. However, after tumor inoculation was determined to be successful at Day 10, the tumorigenic nude mice were randomly divided into seven groups (I: intranasal delivery of saline (n = 8); II: intravenous delivery of saline (n = 8); III: intranasal delivery of free DOX (n = 8); VI: intravenous delivery of free DOX (n = 8); V: intranasal delivery of EVMs@DOX (n = 8); VI: intravenous delivery of EVMs@DOX (n = 8); VII: intranasal delivery of CAR-EVMs@DOX (n = 8); and VIII: intravenous delivery of CAR-EVMs@DOX (n = 8)). The dose of DOX given to the nude mice was 3 mg/kg each time. The doses of EVMs@DOX and CAR-EVMs@DOX given to each nude mouse were calculated according to the amount of loaded DOX to ensure a DOX concentration of 3 mg/kg. Intranasal or intravenous administration of the different agents was carried out every three days for five consecutive administrations. Additionally, the tumor growth inhibition efficacy in each treatment group was monitored by in vivo bioluminescence imaging using an IVIS imaging system (IVIS Spectrum, Caliper) once a week followed by analysis with Live Image 4.4 software (Caliper Life Sciences). The mouse body weights were recorded every 2 days, and their survival status was confirmed each day. At the termination of the in vivo experiments (Day 25), the nude mice in each group (n = 3) were sacrificed according to the standard procedure, and the brain and heart tissues were immediately frozen at −80 °C. Then, 7 μm frozen GBM brain sections from each group were subjected to H&E staining to compare the tumor areas and malignancy. The other nude mice were kept for further survival assessment.

2.12. In vivo evaluation of the cardiotoxicity of CAR-EVMs@DOX

For the cardiotoxicity evaluation, the heart tissue that was obtained from the nude mice after termination of the experiment (Day 25) was immediately frozen at −80 °C and sliced into 7 μm thick sections. Then, the sections were subjected to H&E, TUNEL and DHE staining (Beyotime Biotechnology, China). H&E and DHE staining were performed with the appropriate kits obtained from Beyotime Biotechnology (Shanghai, China). The TUNEL assay was performed with an in situ TUNEL kit (Roche, Switzerland). DAPI was employed to stain cell nuclei. The staining procedures mentioned above were all performed in accordance with the manufacturers' instructions.

After the mice were sacrificed, serum was collected and the concentration of CK-MB and LDH was detected by ELISA kit (Yanjin Biological, China) following the instructions. Briefly, blood was centrifugated 3000 rpm for 30 min after collected. Absorbance at 450 nm wavelength was measured using ELISA kits of CK-MB and LDH respectively, and concentrations of CK-MB and LDH in serum were calculated according to the standard curve.

To measure the apoptosis-related gene expression, heart tissue obtained from the nude mice was used to perform quantitative Polymerase Chain Reaction (qPCR) assay. In brief, cardiomyocyte RNA was extracted by the RNAeasy™ Animal RNA Isolation Kit (Beyotime, China) according to the instructions. Then RNA was reverse transcripted by HiScript III RT SuperMix (Vazyme, China). ChamQ Universal SYBR qPCR Master Mix (Vazyme, China) and primer of Bax, Bcl-2 and GAPDH were used to performed qPCR. The sequence of primers used in the study are listed in Table S2.

2.13. Statistical analysis

All the data in this study were measured in triplicate at least and are presented as the mean ± standard deviation (SD). Statistical variance of two groups was analyzed with Student's *t*-test, statistical variance of Kaplan-Meier plot of the survival study was analyzed with Log-rank test, and statistical variance of multiple groups was analyzed with one- and two-way ANOVA with Bonferroni post hoc tests using SPSS version 16.0 software (SPSS, USA). A p value < 0.05 was considered statistically significant.

3. Results

3.1. Preparation and characterization of CAR-EVMs@DOX

In this study, we constructed a biomimetic intranasal drug delivery nanoplatform to load and deliver the chemotherapeutic drug DOX for GBM treatment. First, EGFRvIII-CAR-modified THP-1 cells were collected and mixed with DOX. Next, CAR-EVMs@DOX was synthesized by serial physical extrusion and purified by ultracentrifugation and washing steps. The extrusion method offers CAR-EVMs@DOX the opportunity to carry membrane-bound EGFRvIII-specific CARs and inherent chemokine receptors from the parental CAR-THP-1 cell membrane to selectively deliver DOX to EGFRvIII-overexpressing GBM cells (Fig. 1a).

To examine the effectiveness of CAR-EVMs@DOX as a drug delivery nanoplatform, a series of tests were performed. Transmission electron microscopy (TEM) demonstrated that synthetic EVMs@DOX and CAR-EVMs@DOX possessed typical phospholipid bilayer-enclosed

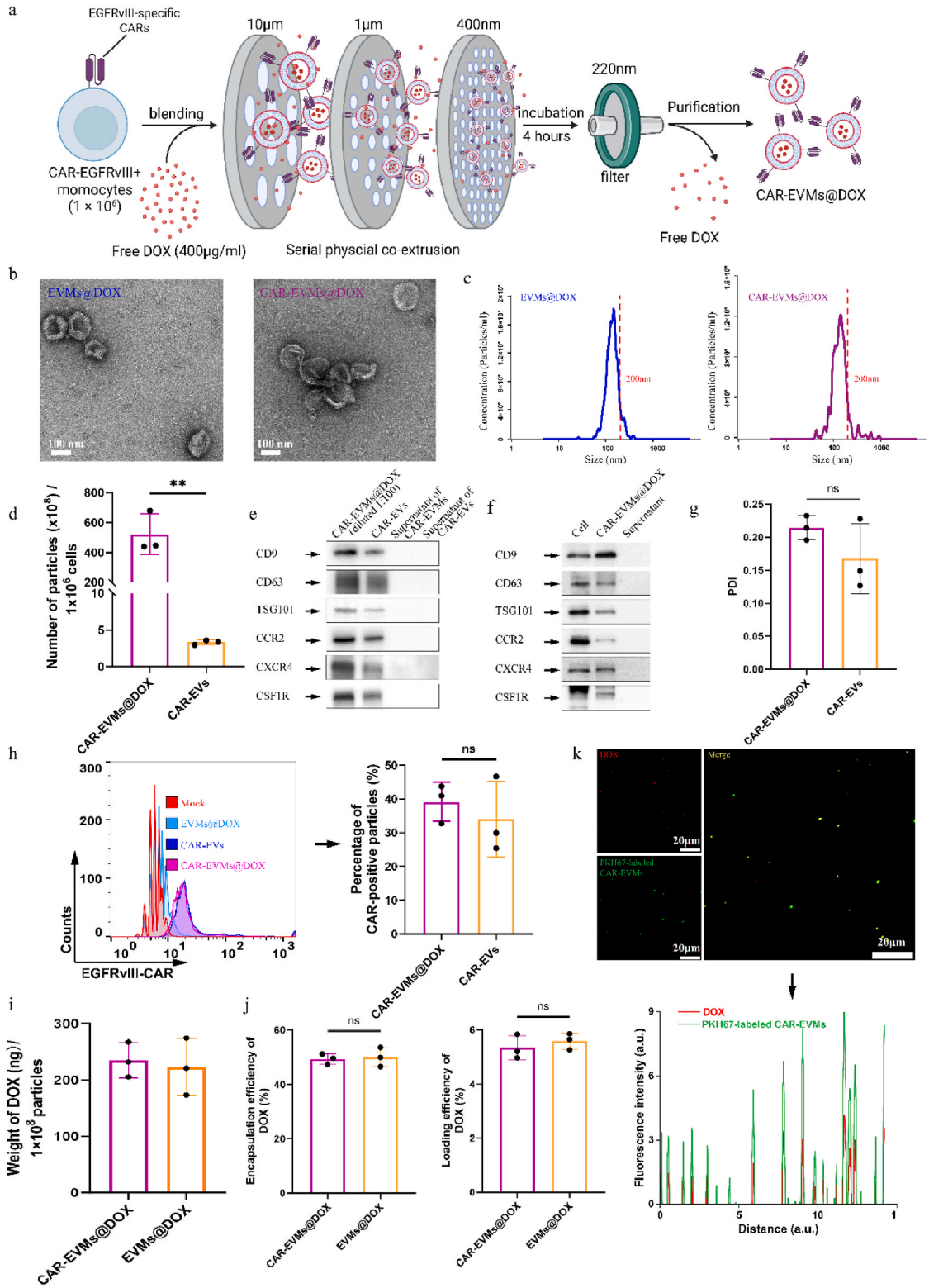

Fig. 1. Characterization of the drug delivery system. a) Schematic diagram of drug-loaded vesicles prepared by physical coextrusion using monocytes and doxorubicin (Created in BioRender. Cheng, Q. (2025) https://BioRender.com/c05d120). **b)** TEM images of EVMs@DOX/CAR-EVM@DOX; Scale bar: the length of white rectangle indicates 100 nm. **c)** Size distribution of EVMs@DOX/CAR-EVM@DOX. **d)** Yield of synthesized CAR-EVMs@DOX and native CAR-EVs from CAR-THP-1 cells (n = 3). **e)** Western blot analysis of CAR-EVMs@DOX (diluted 1:100) and native CAR-EVs derived from 1×10^8 CAR-THP1. **f)** Western blot analysis of EVMs@DOX/CAR-EVMs@DOX. **g)** Polydispersity index (PDI) of CAR-EVMs@DOX and native CAR-EVs (n = 3). **h)** Flow cytometry analysis of CAR-positive percentage in CAR-EVMs@DOX and native CAR-EVs; FITC-conjugated Protein L was used to mark the CAR-positive particles (n = 3). **i)** Drug loading capacity of EVMs@DOX/CAR-EVMs@DOX measured as the weight of DOX per number of particles (n = 3). **j)** Encapsulation efficiency (EE) and loading efficiency (LE) of DOX in EVMs@DOX/CAR-EVM@DOX (n = 3). **k)** Confocal images and colocalization analysis of CAR-EVMs (labeled with PKH67, green) and DOX (red) of CAR-EVMs@DOX; Scale bar: the length of white rectangle indicates 20 μm. Statistical variance was analyzed with Student's *t*-test. *p value < 0.05; **p value < 0.01; ***p value < 0.001; ****p value < 0.0001; ns, not significant.

morphologies (Fig. 1b) that mirrored the classic EV morphology well. In addition, nanoparticle tracking analysis (NTA) revealed that the particle sizes of EVMs@DOX and CAR-EVMs@DOX were less than 200 nm in the majority (Fig. 1c). CAR-EVMs@DOX was obtained by the extrusion method in high yield, as 5.2×10^{10} particles were obtained per 1×10^{6} cells. Notably, compared to native EVs, the yield of synthetic CAR-EVMs@DOX was more than 150-fold higher (Fig. 1d). The Western blot and quantification analysis of EV protein markers on CAR-EVMs@DOX and CAR-EVs also revealed that the yield of CAR-EVMs@DOX was much more than CAR-EVs (Fig. 1e, Fig. S2b). Importantly, use of the extrusion method requires sacrifice of the parental cells to obtain EVMs, but as the native EVs were purified from the supernatant of the culture media, the parental cells could be retained. However, considering the greater yield of EVMs, high proliferation rate of THP-1 cells and EV-free culture media requirement to avoid the presence of external EVs in the culture medium for native EV purification, large-batch production of CAR-EVMs@DOX remained superior. Western blotting demonstrated that the synthesized CAR-EVMs@DOX and native CAR-EVs were enriched with the EV-associated biomarkers CD9, CD63 and TSG101 (Fig. 1f, Fig. S2c) [35,36]. Moreover, polydispersity index (PDI) was assessed by dynamic light scattering. PDI of CAR-EVMs@DOX and CAR-EVs were both lower than 0.25, which showed the size of particles with uniform distribution (Fig. 1g).

As CAR-EVMs@DOX was obtained from CAR-THP-1 cells and increasing evidence has proven that monocyte surface proteins play key roles in signaling and recruitment, three vital GBM-associated chemokine receptors, CC-chemokine receptor 2 (CCR2), C-X-C chemokine receptor 4 (CXCR4) and colony-stimulating factor 1 receptor (CSF1R), were detected at high levels in CAR-EVMs@DOX and native CAR-EVs (Fig. 1f, Fig. S2c). CCR2 is a CC-chemokine ligand 2 (CCL2) receptor that is mainly secreted by GBM cells, microglia and macrophages and recruits myeloid cells to the tumor site through the CCL2-CCR2 interaction [37,38]. CXCR4, a C-X-C chemokine ligand 12 (CXCL12) receptor, and CSF1R, a colony stimulating factor 1 (CSF1) receptor, have been reported to participate in the recruitment of monocytes from blood in response to GBM cells and TAM-secreted CXCL12/CSF1 [39,40]. Thus, the locations of the above surface proteins on CAR-EVMs@DOX offer these nanomedicine opportunities to transfer to the GBM site and lay the foundation for the recognition of CARs by the EGFRvIII antigen.

To detect the location of CARs on CAR-EVMs@DOX, we used FITC-conjugated Protein L to mark the CAR-positive particles. The results revealed that the synthesized CAR-EVMs@DOX exhibited a CAR-positive rate similar to that of native CAR-EVs, demonstrating that CAR-EVMs@DOX maximally retained CARs on the surface and possessed the ability to specifically recognize the corresponding antigen of the CAR structure (Fig. 1h).

The average loading of DOX into CAR-EVMs@DOX and EVMs@DOX was 237.7 ± 24.2 ng and 227.8 ± 55.6 ng, respectively, per 1×10^{8} particles (Fig. 1i). The average loading of DOX in one previous study using the sonication method was 194.6 ± 45.3 ng per 1×10^{8} particles. Previous studies on EVMs mainly encapsulated their intrinsic cargos via sonication, which contributes to efficient encapsulation [2,4,7,41]. However, this method increases the complexity and difficulty of the manufacturing process. In our study, through coextrusion and incubation, CAR-EVMs@DOX revealed an encapsulation efficiency comparable to that obtained in previous studies [15], thus offering a relatively simple method to encapsulate cargos into EVMs.

Based on the standard curve of DOX, EE of DOX in CAR-EVMs@DOX and EVMs@DOX were calculated to be 49.33 ± 1.60 % and 50.06 ± 2.87 %, while LE of DOX in CAR-EVMs@DOX and EVMs@DOX were calculated to be 5.24 ± 0.02 % and 5.69 ± 0.03 %, respectively (Fig. 1j). Fluorescence images revealed that PKH67-labeled CAR-EVMs (green) and DOX (red) mostly overlapped. Moreover, semiquantitative analysis of the images showed that the fluorescence of CAR-EVMs (green) was coupled with that of DOX (red) (Fig. 1k). These results suggested that DOX was successfully loaded into CAR-EVMs@DOX.

Taken together, after analysis by a series of tests, the data show that our synthesized CAR-EVMs@DOX had basic characteristics that were similar to those of native EVs. Moreover, CAR-EVMs@DOX was produced in high yield suitable for mass production, displayed engineered surface proteins for GBM targeting, and had an efficient and simple drug-loading capacity, which may advance its clinical translation for GBM treatment.

3.2. Tumor targetability In vitro and BBB transport

The coating of the CAR-EVMs endowed the final synthesized CAR-EVMs@DOX with the ability to target GBM and penetrate the BBB. A schematic diagram described the processes for evaluating the characteristics of EVMs/CAR-EVMs uptake by cells (Fig. 2a). The characteristic of protein expression of EGFRvIII in U87NC and EGFRvIII-positive U87 cells was shown in Fig. S2d. To analyze the capability of CAR-EVMs to target EGFRvIII-positive GBM (determine EGFRvIII specificity), we first compared the cellular uptake of EVMs and CAR-EVMs by EGFRvIII-positive U87 cells. The fluorescence images showed time-dependent uptake of both EVMs and CAR-EVMs by EGFRvIII-positive U87 cells. In addition, the images revealed that compared to EVMs, significantly more CAR-EVMs were taken up by EGFRvIII-positive U87 cells (Fig. 2b, Fig. S3a–b). The corresponding quantification of the mean fluorescence intensity supported these results, suggesting that the CARs were successfully engineered on the surface of the CAR-EVMs and worked as intended (Fig. 2b).

In addition to amenable tumor-targeting ability, another key issue for therapeutic drugs is reducing their uptake by normal tissue to the greatest extent [42,43]. Thus, we tested CAR-EVMs and EVMs in two normal tissue cell lines, HUVECs and bEnd.3 cells. The results revealed that the uptake of CAR-EVMs and EVMs by HUVECs and bEnd.3 cells was significantly lower than that by EGFRvIII-positive U87 cells (Fig. 2c, Fig. S3c). In addition, compared to that of the EVM-treated EGFRvIII--positive U87 cells, the fluorescence of the CAR-EVM-treated HUVECs and bEnd.3 cells was significantly weaker (Fig. 2c). Moreover, the uptake of CAR-EVMs and EVMs in HOPC cells (human oligodendrocyte precursor cells) was also much lower than EGFRvIII-positive U87 cells (Fig. S3c). This suggests that the EVMs themselves possessed a specific ability to target U87 cells, while CARs enhanced the specific uptake into EGFRvIII-positive U87 cells, further demonstrating that CAR-EVMs could specifically target EGFRvIII-positive GBM.

Previous studies have verified the BBB penetration ability of EVs/EVMs [15,44,45]. Thus, before we administered CAR-EVMs via different routes in vivo, we constructed an in vitro BBB model as previously described to assess whether our CAR-EVMs could pass through the BBB in vitro (Fig. S4a) [4]. As the fluorescence images show, EVMs and CAR-EVMs both penetrated the BBB in a time-dependent manner, which is in agreement with previous studies. Moreover, the bottom EGFRvIII-positive U87 cells took up more CAR-EVMs than EVMs, which could be due to the CAR function (Fig. S4b). To summarize, CAR-EVMs possess an advanced tumor-targeting ability and can pass through the BBB in vitro, which can be attributed to the inherent targeting ability of the parental cells and the engineered surface CAR proteins.

3.3. Drug delivery properties

DOX is a common anthracycline chemotherapeutic agent that is used clinically for the treatment of multiple cancers, including leukemia, lymphoma and many solid tumors [46]. However, DOX fails to pass through the BBB due to its affinity for efflux transporters that are resistant to multiple drugs, thereby limiting its utility in the treatment of brain tumors [47]. Regardless, DOX efficacy against GBM was proven to be nearly 2000-fold greater than that of the standard clinical agent temozolomide in vitro [48]. Therefore, in addition to seeking new chemotherapeutic agents with BBB penetration capacity, it is worth exploring new routes and delivery vesicles to apply existing powerful

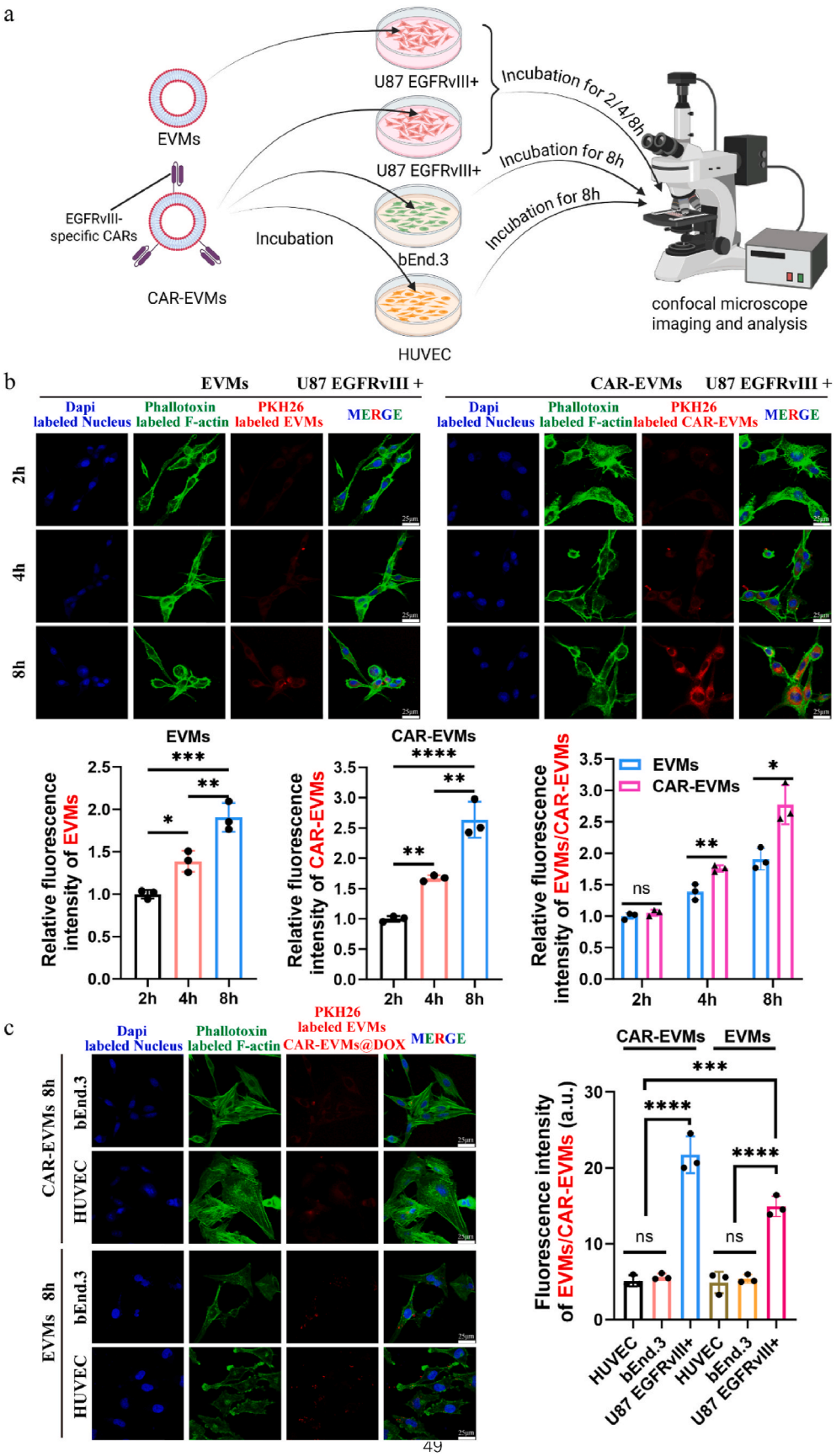

(caption on next page)

Fig. 2. In vitro tumor targetability of the EVMs-based drug delivery platform. a) Schematic diagram for evaluating the characteristics of EVMs/CAR-EVMs uptake by cells (Created in BioRender. Cheng, Q. (2025) https://BioRender.com/y48m203). **b)** Confocal images and quantification analysis of the EVMs/CAR-EVMs uptake by the EGFRvIII-positive U87 cells after incubation of 2, 4, 8 h (n = 3); Scale bar: 25 μm. **c)** Confocal images and quantification analysis of the EVMs/CAR-EVMs uptake by the bEnd.3 cells and HUVECs after incubation of 8 h (n = 3); Scale bar: the length of white rectangle indicates 25 μm. DAPI (blue) labeled nucleus, PKH26 (red) labeled EVMs/CAR-EVMs and Alexa Fluor 488-conjugated phalloidin (green) labeled F-actin. Statistical variance was analyzed with Student's *t*-test (two groups) and one-way ANOVA (multiple groups). *p value < 0.05; **p value < 0.01; ***p value < 0.001; ****p value < 0.0001; ns, not significant.

therapeutic agents.

Based on this, we assessed the DOX delivery properties of EVMs@-DOX and CAR-EVMs@DOX in vitro before carrying out animal experiments. In order to verify the efficiency of DOX loaded nanoparticles, CCK8 assay was performed to detect the variability of U87NC and EGFRvIII-positive U87 cells. The results showed that after 8 h of incubation with equal amounts, there was no significant difference in the inhibition of U87NC by CAR-EVMs@DOX and EVMs@DOX. While the viability of EGFRvIII-positive U87 cells incubated with CAR-EVM@DOX was significantly lower than that of the EVMs@DOX group (Fig. 3a). In addition, the results of clonal formation and flow cytometry were consistent with the above results (Fig. 3b). To clarify the reasons for a decrease of viability, the expression of apoptosis-related proteins in each group was analyzed by Western blot (Fig. 3c). The effect of CAR-EVMs@DOX on inducing apoptosis of EGFRvIII-positive U87 cells was the strongest and significantly different from EVMs@DOX (Fig. 3d–e). However, free DOX exhibited significantly cytotoxicity within 8 h incubated with U87NC and U87EG compared to EVMs@DOX/CAR-EVMs@DOX. This difference is primarily attributed to the distinct cellular uptake and drug release mechanisms of the two formulations. Multiple researches referred that due to EVMs release delay and high toxicity of free DOX, free DOX is more toxic in a short time [49–52]. Therefore, the structure of EVMs weakened the short-term toxicity of free DOX.

EGFRvIII-positive U87 cells represented more sensitive to CAR-EVM@DOX compared with U87NC. Conversely, the anti-tumor effect of EVM@DOX in two kinds of cells was similar. Since free DOX is able to induce apoptosis of various tumor cells such as U87MG, we believe that apoptosis of EGFRvIII-positive U87 cells is mainly due to the more efficient DOX delivery into cells [46,53]. To verify this hypothesis, fluorescence confocal microscopy was used to compare the DOX delivery efficiency between CAR-EVMs@DOX and EVMs@DOX.

As shown in Fig. 3f, compared to EVMs@DOX treatment, CAR-EVMs@DOX-treated EGFRvIII-positive U87 cells exhibited significantly stronger green and red fluorescence, which represents PKH67-labeled CAR-EVMs@DOX, EVMs@DOX and DOX, respectively (Fig. 3f, Fig. S5a–b). Additionally, these results were supported by the corresponding quantification of mean fluorescence intensity (Fig. 3g–h).

Notably, although less EVMs@DOX was taken up by EGFRvIII-positive U87 cells than CAR-EVMs@DOX, the uptake of EVMs@DOX was considerable, further supporting that CAR-EVMs@DOX, with the combined targeting abilities received inherently from the parental cells and via the engineered surface CAR proteins, was equipped with antigen-specific properties for efficient DOX delivery to cancer cells.

3.4. *In vivo tumor targeting and cardiac distribution study*

Next, the tumor-targeting capacities of CAR-EVMs@DOX and EVMs@DOX were analyzed using an intracranial EGFRvIII-positive GBM mouse model. DiR-labeled CAR-EVMs@DOX/EVMs@DOX or free DiR was administered intranasally to tumor-bearing mice, and the mice were observed at different time points after compound administration using an in vivo spectrum imaging system (IVIS). Additionally, equivalent amount of EVMs@DOX/CAR-EVMs@DOX or free DiR was administered via tail vein injection to the other groups of GBM model mice to compare the intranasal and intravenous targeting efficiencies (Fig. 4a). The approximate location of the tumor is marked with a black circle according to the bioluminescence images obtained from the IVIS imaging system. As Fig. 4b shows, due to its mucoadhesive nature, DiR-labeled CAR-EVMs@DOX mainly accumulated in the nasal cavity at first and then revealed time-dependent migration toward the brain tumor site.

As time passed, the CAR-EVMs@DOX was absorbed through the nasal mucosa, migrated through the trigeminal and olfactory nerve branches into the brain, and was finally recruited into the tumor site [54,55].

In addition, intranasal administration of DiR alone and intravenous administration of three treatments exhibited little fluorescence in the tumor site, while CAR-EVMs@DOX administered via the intranasal route exhibited the highest accumulation in the tumor location among all groups, suggesting that CAR-EVMs@DOX could efficiently migrate and accumulate in EGFRvIII-positive GBM sites. Moreover, compared to intravenous administration, CAR-EVMs@DOX and EVMs@DOX administered via the intranasal route accumulated higher than intravenous route in tumor region. In particular, intranasal administration of CAR-EVMs@DOX exhibited an earlier peak arrival time (8 h) and higher accumulation at the tumor site, which demonstrated that intranasal administration of this engineered tumor-targeting nanoplatform is advanced and highly efficient for brain tumor treatment. It is worth mentioning that although the tumor location was marked according to the bioluminescence images, the actual successful migration of CAR-EVMs@DOX into the brain was hard to define in the living animal images.

Thus, the exceptional capacity to target tumors in the brain was further verified by ex vivo imaging of brain tissue from mice sacrificed 24 h postadministration (Fig. 4c–d, Fig. S6). As shown in Fig. 4c and d, mice treated with CAR-EVMs@DOX intranasally exhibited the overall highest DiR fluorescence signal, whereas free DiR-treated mice exhibited the overall lowest fluorescence signal, which was in accordance with the in vivo fluorescence images. Notably, the mice treated with CAR-EVMs@DOX via tail vein injection showed a higher fluorescence signal than those treated with EVMs@DOX intranasally and intravenously, a result that differed from the in vivo imaging data. Considering that ex vivo brain tissue imaging is a visual observation method, these results could be more in line with the actual physiological conditions, which further confirmed that CAR-EVMs@DOX possessed the abilities of specific targeting and superb migration to EGFRvIII-positive GBM.

In clinical applications, DOX is mainly injected intravenously or used as a liposome-encapsulated injectable formulation [56]. Despite its powerful anticancer abilities, the administration of DOX is mainly restricted by its serious cardiotoxicity [57]. The symptoms of DOX-induced cardiotoxicity mainly manifest as arrhythmia, cardiomyopathy and congestive heart failure [58]. Hence, the enrichment of the DOX-loaded nanoagents in the heart was evaluated via ex vivo imaging of heart tissue from mice sacrificed 24 h after intranasal/intravenous administration (Fig. 4c–d, Fig. S6). As shown in Fig. 4c and d, weak fluorescence was observed in the hearts of mice treated with free DiR and those intranasally administered DiR-labeled EVMs@DOX, and negligible fluorescence was observed in the intranasal CAR-EVMs@DOX-treated group. In contrast, intravenous administration of EVMs@DOX and CAR-EVMs@DOX resulted in obviously more accumulation in the heart than intranasal administration, which verified that intranasal administration of CAR-EVMs@DOX could superbly protect against DOX-induced cardiotoxicity.

Next, we analyzed the particles distribution in the brains of mice with EGFRvIII-positive GBM that were sacrificed 24 h after intranasal

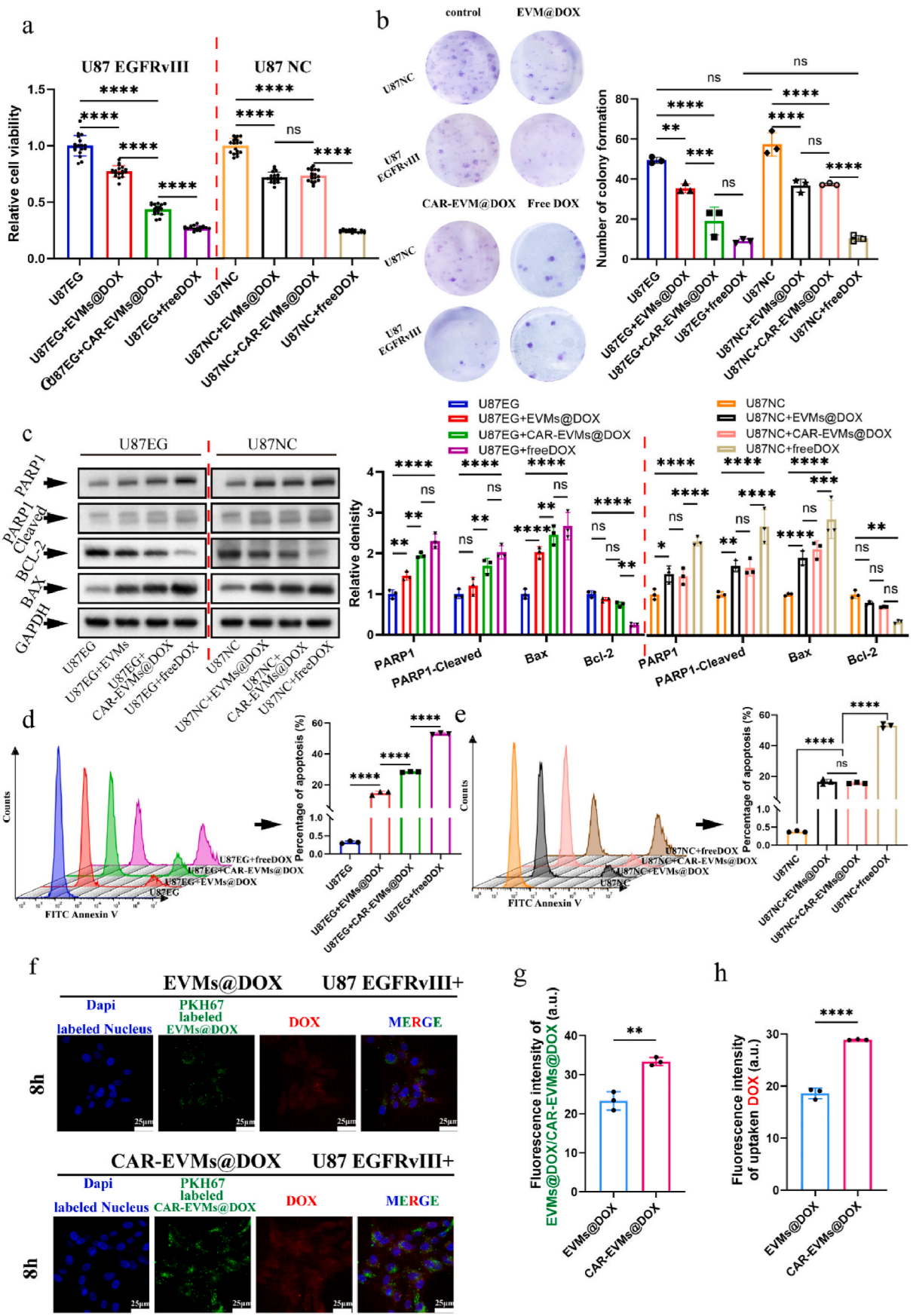

(caption on next page)

Fig. 3. In vitro drug delivery properties of the drug delivery system. a) CCK8 assay shows the relative viability of U87 EGFRvIII positive cells (U87EG) and U87 negative control cells (U87 NC). Data was normalized by groups of U87NC and U87EG (n = 18). **b)** Clonal formation and quantification analysis of U87 NC and U87EG in four treatments (added DMEM culture medium, EVMs@DOX,CAR-EVMs@DOX and freeDOX respectively, n = 3). **c)** Apoptosis-related protein bands of U87NC cells and U87EG tasted by Western blot and quantification analysis for each band. Data was normalized by groups of U87NC and U87EG (n = 3). **d-e)** Flow cytometry and quantification analysis of the apoptosis of U87EG and U87NC; FITC-conjugated Annexin V was used to marked the apoptotic cells (n = 3). **f)** Confocal images of the EVMs@DOX/CAR-EVMs@DOX uptake by the EGFRvIII-positive U87 cells after incubation of 8 h; Scale bar: the length of white rectangle indicates 50 μm; DOX (red); DAPI (blue) labeled nucleus and PKH67 (green) labeled EVMs@DOX/CAR-EVMs@DOX. **g-h)** Quantification analysis of the PKH67 (green fluorescence) and DOX (red fluorescence) uptake that labeled EVMs@DOX/CAR-EVMs@DOX by the EGFRvIII-positive U87 cells after incubation of 8 h (n = 3). Statistical variance was analyzed with Student's *t*-test (two groups) and one-way ANOVA (multiple groups). *p value < 0.05; **p value < 0.01; ***p value < 0.001; ****p value < 0.0001; ns, not significant.

administration of EVMs@DOX/CAR-EVMs@DOX or free DiR. Encouragingly, images of the EGFRvIII-positive GBM brains had significantly higher CAR-EVMs@DOX accumulation in the tumor site than in the normal tissue, and negligible signals from CAR-EVMs@DOX were observed in the normal tissue sites (Fig. 4e).Furthermore, there was no significant difference between fluorescence of EVMs@DOX in the tumor site and normal tissue (Fig. S7). In summary, these data support our hypothesis that CAR-EVMs@DOX possesses a superb and specific EGFRvIII-positive GBM-targeting capacity and may reduce DOX-induced cardiotoxicity.

3.5. Antitumor effect In vivo

The in vivo therapeutic effect of CAR-EVMs@DOX was analyzed using the intracranial EGFRvIII-positive GBM mouse model, and a schematic of the workflow is shown in Fig. 5a. Ten days after GBM inoculation, different treatments administered either intranasally or intravenously were given to mice every three days for five consecutive treatments. Tumor growth was measured every seven days via in vivo imaging using an IVIS imaging system and reflected by the bioluminescence intensity. As shown in Fig. 5b and c, mice treated intranasally with CAR-EVMs@DOX exhibited significantly more efficient GBM growth inhibition than the other groups. Despite not being administered intranasally, intravenous injection of CAR-EVMs@DOX also produced significant GBM growth inhibition and better than intravenous injection of EVMs@DOX. Then the efficacy of intranasal EVMs@DOX ranked third, which was in line with the results of the in vivo targeting ability tests. In contrast, although present, limited GBM growth inhibition was observed after intranasal and intravenous treatment with free DOX.

In addition, a negligible body weight decline was observed for the mice in the intranasal CAR-EVMs@DOX group. Comparatively, mice treated with saline, free DOX, EVMs@DOX and intravenous CAR-EVMs@DOX exhibited varying degrees of weight decline (Fig. 5d). The weight decline could be attributed to two main factors, brain dysfunction caused by GBM proliferation and systemic toxicity, particularly cardiotoxicity, induced by DOX. These data also aligned with the finding that intranasal administration of CAR-EVMs@DOX enhances the amount of DOX transported to the tumor site and concurrently reduces the systemic toxicity induced by DOX compared to intravenous administration.

In terms of survival time, the median survival time of mice in the intranasal CAR-EVMs@DOX group was 37 days, which was significantly longer than that of mice in the intranasal saline (25 days), intravenous saline (24 days), intranasal free DOX (27 days), intravenous free DOX (24 days), intranasal EVMs@DOX (30 days), intravenous EVMs@DOX (28.5) and intravenous CAR-EVMs@DOX groups (33 days) (Fig. 5e).

Next, hematoxylin and eosin (H&E) staining was performed to analyze the histology of the GBM mouse brains, and the section of each sample with the largest tumor area is shown. As displayed in Fig. 5f, the H&E staining results revealed that mice intranasally administered CAR-EVMs@DOX exhibited a significantly smaller tumor area, which further confirmed that intranasal CAR-EVMs@DOX administration efficiently inhibited tumor growth.

Together, these results reconfirm that intranasal administration of CAR-EVMs@DOX offers a highly safe and reliable method to deliver powerful therapeutic agents into the GBM site for efficient antitumor efficacy.

3.6. In vivo protection against DOX-induced cardiotoxicity

The enrichment of intranasally administered CAR-EVMs@DOX in the heart was proven to be negligible in mice sacrificed 24 h after administration (Fig. 4c–d). We further analyzed the protective effects of CAR-EVMs@DOX against DOX-induced cardiotoxicity during the therapeutic process. In terms of cardiac muscle morphology, the results of H&E staining showed that mice treated with free DOX intranasally/intravenously and with CAR-EVMs@DOX intravenously had significantly lower cardiomyocyte density and enhanced nuclear chromatin condensation, which indicated cardiotoxicity. In contrast, not including the intranasal saline group, the fewest changes in cardiomyocytes were observed in the intranasal CAR-EVMs@DOX group (Fig. 6a, Fig. S8a). As DOX has been proven to stimulate the generation and accumulation of reactive oxygen species (ROS) and induce apoptosis in cardiomyocytes [59–61], cumulative ROS levels and apoptosis were assessed by examining histological sections. ROS accumulation and apoptosis levels were determined by dihydroethidium (DHE) and TUNEL fluorescence, respectively (Fig. 6a, Fig. S7b–c). The results revealed that intranasally delivered CAR-EVMs@DOX dramatically reduced the cumulative ROS levels and degree of apoptosis that accompanies DOX-induced cardiotoxicity (Fig. 6b–c). Meanwhile, ELISA assay was used to detect LDH and CK-MB in the blood of mice to estimate the severity of myocardial injury. The results were consistent with the histological sections of myocardium (Fig. 6d–e). DOX has shown inducing myocardial cell damage by apoptosis [62–64]. Thus, we compared the mRNA expression of apoptosis-related genes in myocardial tissue of mice in different treatment groups. Bax and Bcl-2 are the key genes regulating apoptosis, and the increase of the mRNA ratio of Bax to Bcl-2 indicates the activation of apoptosis pathway. We observed that the apoptosis of cardiomyocytes was similar to the above experimental results (Fig. 6f–g). Apparently, intranasal administration shows lower cardiotoxicity compared to intravenous administration. On the other hand, under the same administration mode, CAR-EVMs@DOX can be more effective in reducing cardiac toxicity. Notably, these histological results concurrently revealed that compared to intravenous administration, intranasal delivery of nanoagents may emerge as a more secure tactic to circumvent peripheral systemic toxicity for brain tumor treatment.

In summary, these data verified that intranasal administration of CAR-EVMs@DOX was a feasible tactic to reduce the cardiotoxicity of encapsulated DOX.

4. Discussion

Recently, an increasing number of studies have explored the brain delivery potential of native EVs [65,66]. Despite various breakthroughs, the application of native EVs remains limited by their poor yield and tedious workflow. As a solution, EVMs with exceptionally high yields and relatively low costs have emerged as a research hotspot, and previous studies have demonstrated that EVMs have characteristics and targeting abilities that are similar to those of native EVs [19,67,68]. In our study, we successfully synthesized CAR-EVMs@DOX in high yield

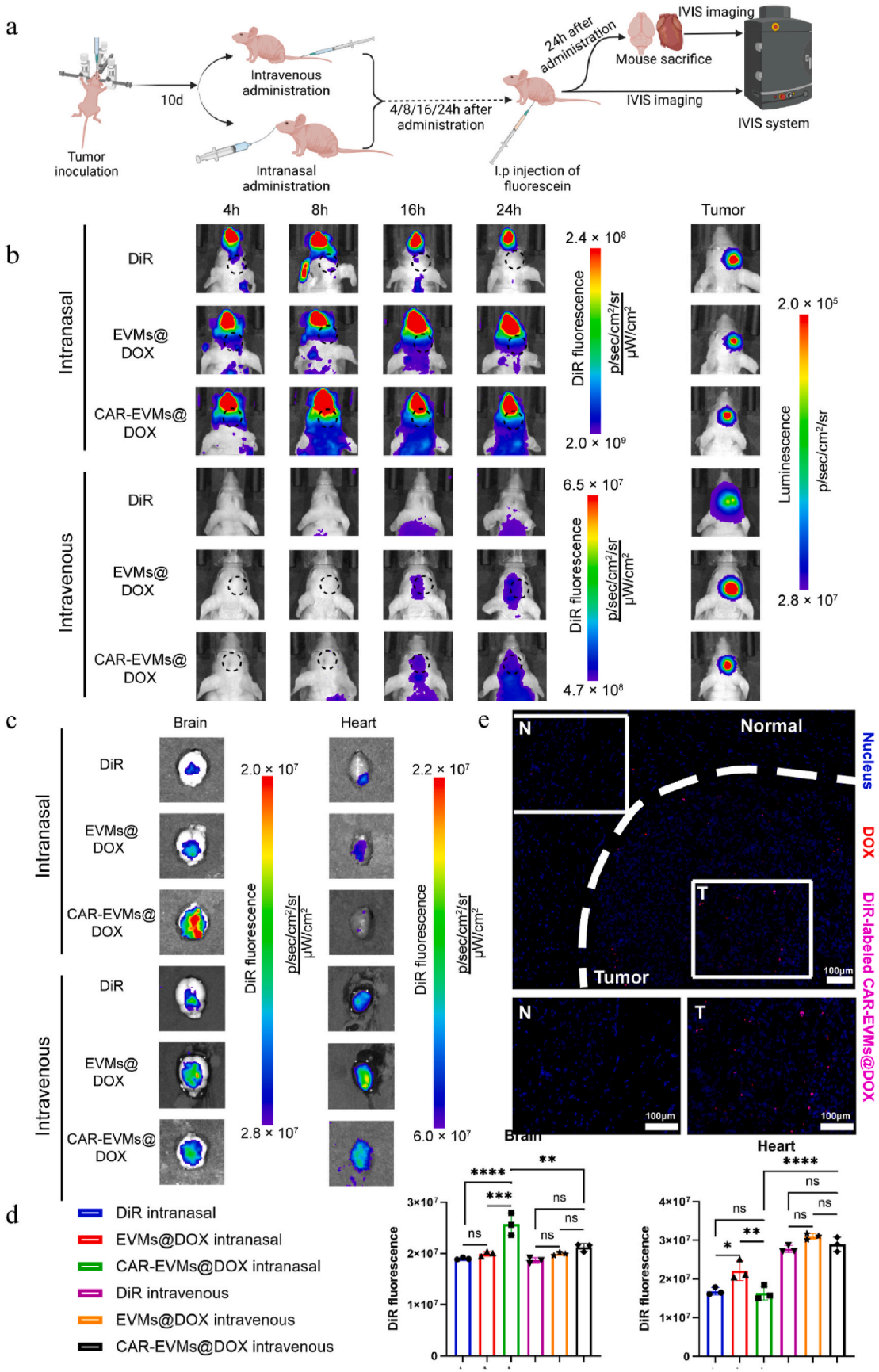

(caption on next page)

Fig. 4. In vivo tumor targeting and cardiac distribution analysis. a) Schematic illustration of the procedures for evaluating tumor targeting and cardiac distribution (Created in BioRender. Cheng, Q. (2025) https://BioRender.com/u63h983). **b)** In vivo fluorescence tracking of DiR or DiR-labeled nanoagents tumor accumulation and in vivo bioluminescence images of nude mice bearing EGFRvIII-positive GBM. The black circles in in vivo fluorescence images marked the approximate location of the tumor. **c)** Ex vivo fluorescence images of DiR or DiR-labeled nanoagents in brain and heart tissues from nude mice 24 h post-administration of CAR-EVMs@DOX. **d)** Fluorescence intensity quantification of Dir or DiR-labeled nanoagents in brain and heart tissues (n = 3). **e)** Confocal images of brain section from intranasal CAR-EVMs@DOX administration group 24 h postadministration; Scale bar: the length of white rectangle indicates 100 μm; N: normal site, T: tumor site; DOX (red); DAPI (blue) labeled nucleus and DiR (pink) labeled CAR-EVMs@DOX. Statistical variance was analyzed with one-way ANOVA. *p value < 0.05; **p value < 0.01; ***p value < 0.001; ****p value < 0.0001; ns, not significant.

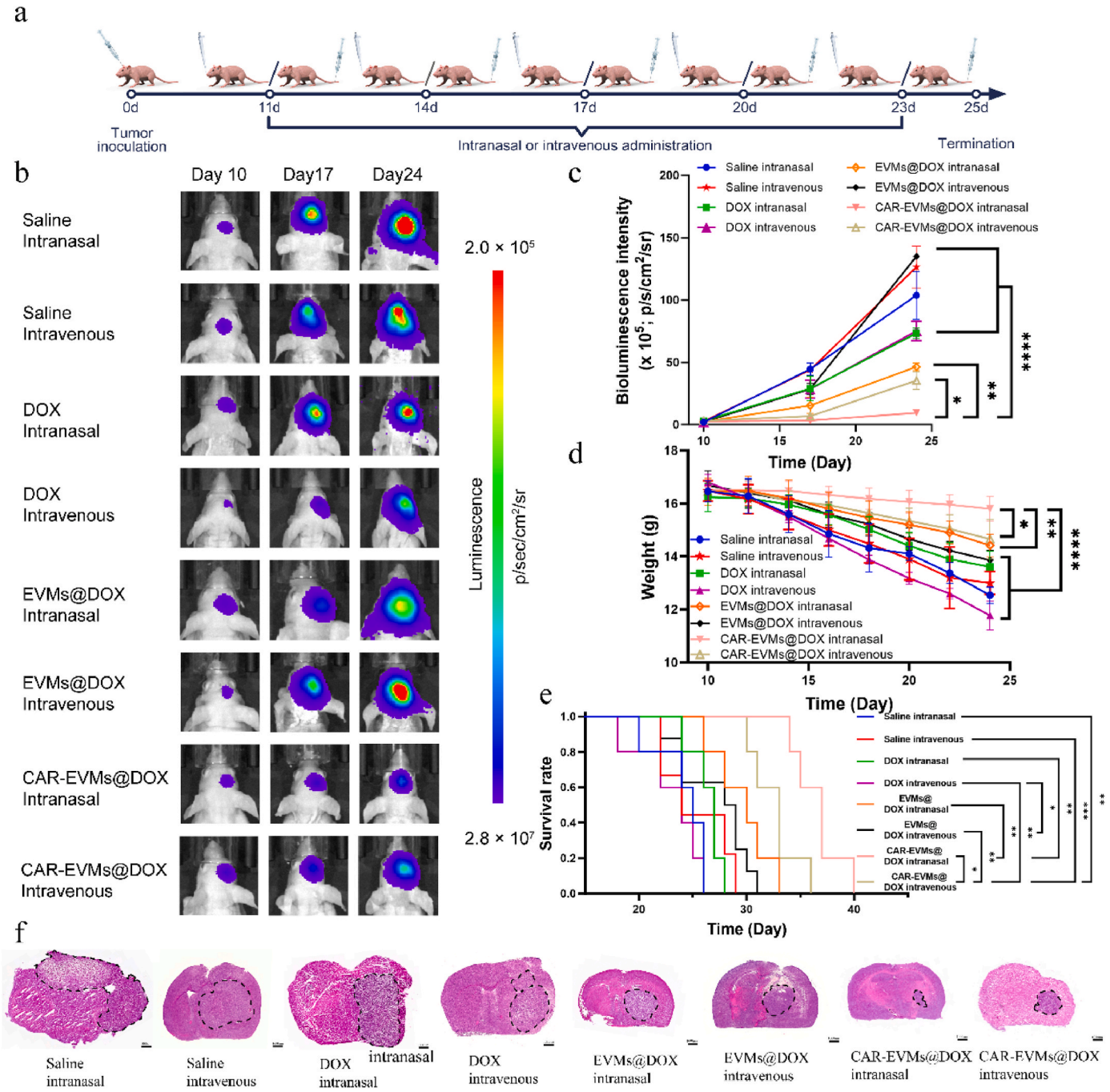

Fig. 5. In vivo anti-tumor effects of the drug delivery system using orthotropic GBM models. a) Schematic illustration of the treatment process with nude mice models bearing EGFRvIII-positive GBM. **b)** Representative in vivo bioluminescence images indicating the tumor size in each treatment group. **c)** Bioluminescence intensity quantification curve of the different treatment groups (n = 3). **d)** Body weight changes of the different treatment groups (n = 5). **e)** Kaplan-Meier survival curve of the different treatment groups (n = 5). **f)** H&E staining of the whole brain section and relative tumor area in different treatment groups at the termination point (day 25). The black dotted circles marked the tumor area. Scale bar: the length of black rectangle indicates 1000 μm. Statistical variance was analyzed with one-way ANOVA (bioluminescence intensity and weight on day 25) and Kaplan-Meier plot of the survival study was analyzed with Log-rank test. *p value < 0.05; **p value < 0.01; ***p value < 0.001; ****p value < 0.0001; ns, not significant.

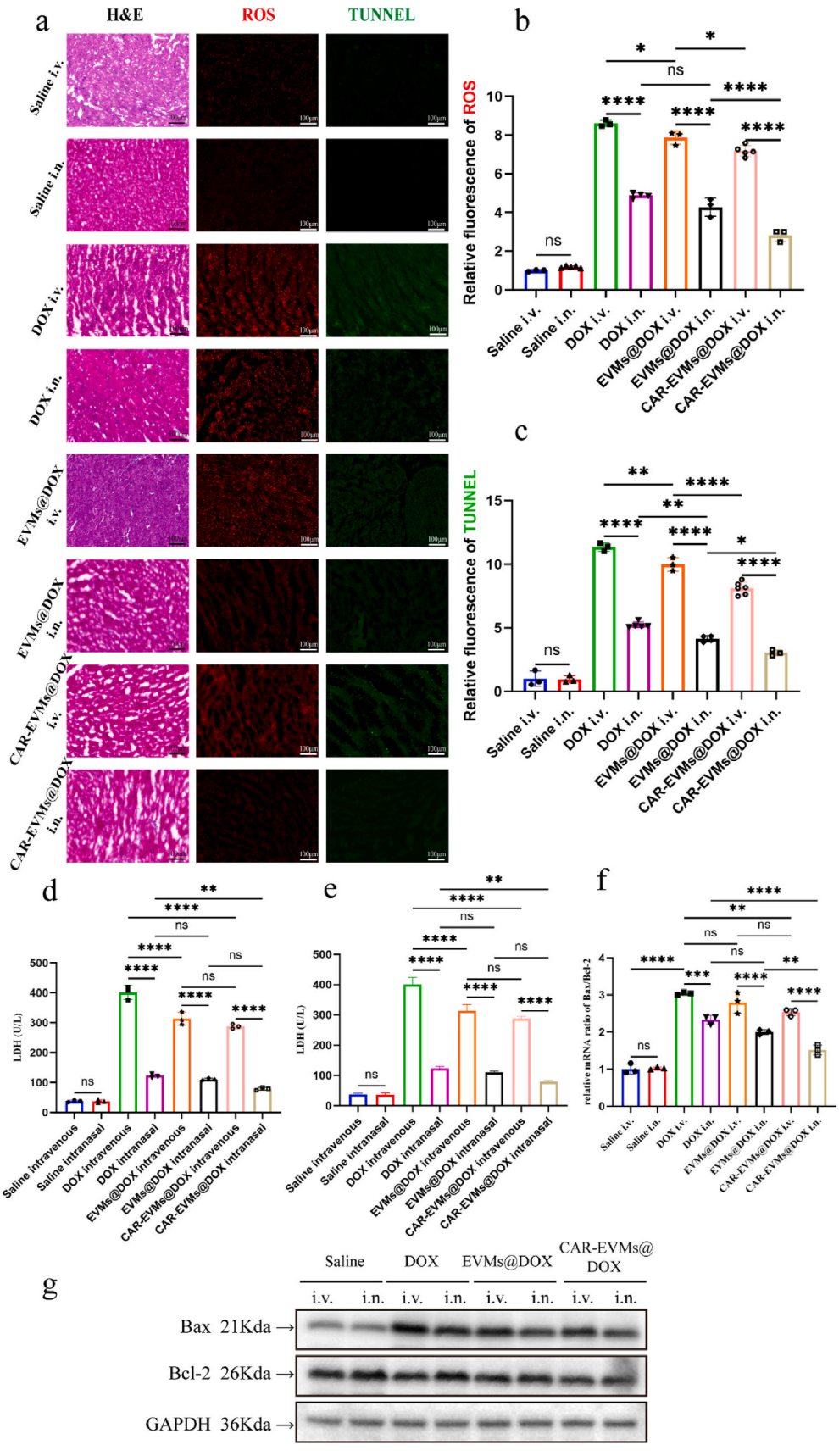

(caption on next page)

Fig. 6. In vivo evaluation of the cardiotoxicity of the drug delivery system. a) H&E staining of the heart tissues in different treatment groups at the termination point (day 25). DHE staining (red) of the heart tissues indicating the ROS accumulation in different treatment groups (day 25). TUNEL staining (green) of the heart tissues indicating the apoptosis in cardiomyocytes (day 25); Scale bar: the length of white rectangle indicates 100 μm. **b-c)** Quantification analysis (n = 3) of the ROS (red fluorescence) and TUNNEL (green fluorescence). **d-e)** ELISA assay shows the concentration of CK-MB and LDH in mice plasma which indicate the damage of cardiomyocyte (day 25, n = 3). **f)** qPCR assay shows the relative mRNA ratio of Bax/Bcl-2 in each treatment groups cardiomyocyte (day 25, n = 3). **g)** The expression of Bax, Bcl-2 and GAPDH in cardiomyocyte performed by Western blot for each treatment groups (day 25). Statistical variance was analyzed with one-way ANOVA. *p value < 0.05; **p value < 0.01; ***p value < 0.001; ****p value < 0.0001; ns, not significant.

via mechanical extrusion and verified its specific GBM-targeting abilities both in vitro and in vivo. To maximize the engineered targeting ability and reduce the undesired uptake by normal tissue to the greatest extent, we employed a dual-targeting design combining the specific recognition ability of CARs with the inherent GBM tropism capacity of monocytes. Notably, although EVMs@DOX was not engineered with CARs, it exhibited background targeting and therapeutic capacity against EGFRvIII-positive GBM, which confirms that this dual-targeting design is a feasible tactic. Moreover, due to the highly editable attributes of CARs for almost all natural antigens, this dual-targeting tactic offers new insight into the treatment of tumor patients with one or more tumor-associated targets and is not restricted to a concrete target. In current GBM treatment, most therapeutic agents are intravenously administered through the peripheral venous system. However, due to the intact BBB, nearly 98 % of these therapeutic agents are not allowed access to brain tumor locations [69]. Intranasal drug delivery, as a route that administers the drug from the nose to the brain via nerve branches, has been proven to be a superb strategy for EV delivery to the brain [33]. Because this route bypasses but does not penetrate the BBB, intranasal delivery offers a completely new approach for more efficient drug delivery to treat CNS disorders. Another vital strength of intranasal EV delivery is that it avoids the direct processes that occur in peripheral blood, thus significantly reducing serum degradation, biological elimination and accumulation in non-CNS organs, which may cause undesired side effects [17]. In our study, intranasal delivery of CAR-EVMs@DOX led to dramatically higher accumulation of the nanomedicine in the GBM site and better protective effects against DOX-induced cardiotoxicity than intravenous delivery. Thus, our study confirms that, as EV alternatives, EVMs delivered intranasally possess the strengths of intranasally delivered EVs.

However, there are some insufficiencies in our study that need to be explored. First, due to their intrinsic inability to load DOX into native EVs via the same mechanical extrusion procedure, native CAR-EVs loaded with DOX (CAR-EVs@DOX) were not analyzed in this study. In addition, we adopted only the EGFRvIII antigen as the model target. Although different CARs recognize their targets via scFvs, it is necessary to attempt to target different GBM-associated targets or combinations of multiple targets to achieve better therapeutic efficacy for brain tumor treatment in the clinic. Moreover, as a nanoplatform dual-targeting GBM, the targeting ability of EVMs derived from monocytes or CARs was not evaluated. As a consequence, the synergy between these factors was not confirmed in depth in our research, and more research is urgently needed to seek the optimal combination. However, our research demonstrated that both CARs and EVMs derived from monocytes contributed to the successful migration of CAR-EVMs@DOX into the GBM site. Meanwhile, the superb improvements of CAR-EVMs@DOX administered intranasally shown in antitumor effect and animal survival time in vivo experiments reconfirmed the efficacy of the dual-targeting nanoplatform.

In addition, this study primarily evaluated the targeting capability of CAR-EVMs@DOX by comparing their delivery efficiency and therapeutic efficacy against those of non-targeted EVMs@DOX. Due to the significant differences in membrane composition, surface modification, particle size, and drug loading capacity between the clinically approved doxorubicin liposomes and the THP-1-derived EVMs/CAR-EVMs developed in this study, we were unable to identify a suitable method to incorporate these commercial formulations into a direct comparative control group. As a future research direction, it is necessary to comprehensively evaluate the pharmacokinetic properties of EVMs and CAR-EVMs—including in vivo release kinetics, circulation half-life, and intratumoral drug delivery efficiency—and benchmark them against mainstream clinically used doxorubicin liposomal formulations, such as Doxil®, Myocet®, and LipoDox®, to further assess their potential for clinical translation [51,70]. Moreover, EVMs derived from THP-1 cells have been reported to possess higher tissue affinity and tumor-targeting ability than synthetic liposomes, rendering EVMs@DOX a more promising platform for glioma therapy [20,71].

However, this study did not include a long-term safety and immunogenicity assessment, partly due to the short survival duration of the in situ glioma mouse model. According to current researches, repeated intranasal administration of DOX may cause cumulative damage to the nasal mucosa and olfactory epithelium [72]. In addition, although CAR modification improves targeting precision, CAR-EVMs@DOX may still release DOX in non-tumor brain regions, such as the hippocampus and olfactory bulb, which are first-exposed areas via the intranasal route [73,74]. Furthermore, the use of incompletely humanized CAR antibody fragments may induce anti-drug antibody responses or immune rejection in clinical settings [75,76]. However, since the mice used in our model are immunodeficient nude mice, they cannot adequately reflect potential immune responses to CAR-modified vesicles in humans.

Therefore, further studies are necessary to evaluate the long-term safety, biodistribution, and immunogenicity of CAR-EVMs@DOX, particularly under chronic administration conditions. Nevertheless, the structural design of CAR-EVMs, which restricts non-specific DOX release, supports their continued investigation as a safe and tumor-targeted intranasal therapeutic strategy for glioblastoma [51].

5. Conclusion

GBM remains incurable, demonstrating that traditional surgical debulking alone is insufficient as a cure. Responses of GBM to standard-of-care therapies, including chemoradiotherapy, are transient, and drugs usually become stuck in the narrow margin around the initial lesion. Applications of EVs/EVMs for tumor therapy have focused on how to increase the tumor-targeting ability while minimizing uptake by other organs to the greatest extent. In this study, a novel GBM-targeting drug delivery nanoplatform, CAR-EVMs@DOX, was synthesized via mechanical extrusion and evaluated after intranasal administration as a targeted GBM therapy. The coextrusion method successfully loaded DOX into CAR-EVMs and endowed the nanoagents with superior GBM dual-targeting ability. In addition, the extrusion method is likely to achieve the encapsulation and targeted delivery of various therapeutic agents, which are not restricted to chemotherapeutic agents. After intranasal administration, the nanoplatform bypassed the BBB and exhibited higher targeted delivery efficiency to the GBM site, which concurrently reduced DOX-induced cardiotoxicity compared with intravenous administration. Taken together, our study results demonstrated the advanced GBM-targeting ability, tumor inhibition efficacy and cardioprotective effects of intranasally administered CAR-EVMs@DOX for GBM treatment, and the strategy to deliver EVM-based nanoplatforms via the intranasal route can potentially advance its future clinical translation.

CRediT authorship contribution statement

Qihong Cheng: Writing – review & editing, Writing – original draft,

Visualization, Methodology, Conceptualization. **Minjie Wang:** Supervision, Data curation, Conceptualization. **Zijie Zhou:** Writing – review & editing, Writing – original draft, Methodology, Conceptualization. **Huitang Xia:** Supervision, Funding acquisition. **Shaojie Yu:** Visualization, Methodology. **Jianglin Zheng:** Methodology. **Kai Zhu:** Visualization, Methodology. **Xudong Li:** Methodology. **Xuan Wang:** Supervision, Funding acquisition. **Tao Xin:** Supervision, Funding acquisition. **Xiaobing Jiang:** Supervision, Funding acquisition. **Junjun Li:** Writing – review & editing, Supervision, Project administration, Funding acquisition.

Ethics approval and consent to participate

The animal experimental protocol in this study was established and approved by the Ethics Committee of Huazhong University of Science and Technology (No. 2022–3008).

Declaration of competing interest

All the authors declare no conflict of interest.

Acknowledgements

This work was supported by the Taishan Scholar Program of Shandong Province [grant numbers: tsqn202312359]; the Scientific Research Cultivation Project in Emerging Strategic Fields [grant numbers: 202403]; the Natural Science Foundation of Hubei Province [grant numbers: 2023AFB596] and the Youth Fund of the National Natural Science Foundation of China [grant numbers: 82203140].

We thank Home for Researchers editorial team (www.home-for-researchers.com) for language editing service.

ABBREVIATIONS

EVs	extracellular vesicles
GBM	glioblastoma
EVMs	extracellular vesicle mimetics
CARs	chimeric antigen receptors
DOX	doxorubicin
BBB	blood−brain barrier
CNS	central nervous system
OS	overall survival
TAMs	tumor-associated macrophages
TME	tumor microenvironment
scFvs	single-chain variable fragments
EGFRvIII	epidermal growth factor receptor variant III
TEM	transmission electron microscopy
NTA	nanoparticle tracking analysis
CCR2	CC-chemokine receptor 2
CXCR4	C-X-C chemokine receptor 4
CSF1R	colony-stimulating factor 1 receptor
CCL2	CC-chemokine ligand 2
CXCL12	C-X-C chemokine ligand 12
IVIS	in vivo spectrum imaging system

Appendix A. Supplementary data

Supplementary data to this article can be found online at https://doi.org/10.1016/j.bioactmat.2025.05.032.

References

[1] Q.T. Ostrom, L. Bauchet, F.G. Davis, I. Deltour, J.L. Fisher, C.E. Langer, M. Pekmezci, J.A. Schwartzbaum, M.C. Turner, K.M. Walsh, et al., The epidemiology of glioma in adults: a "state of the science" review, Neuro Oncol. 16 (2014) 896–913.

[2] T. Wu, Y. Liu, Y. Cao, Z. Liu, Engineering macrophage exosome disguised biodegradable nanoplatform for enhanced sonodynamic therapy of glioblastoma, Adv. Mater. 34 (2022) e2110364.

[3] R. Stupp, M.E. Hegi, W.P. Mason, M.J. van den Bent, M.J. Taphoorn, R.C. Janzer, S. K. Ludwin, A. Allgeier, B. Fisher, K. Belanger, et al., Effects of radiotherapy with concomitant and adjuvant temozolomide versus radiotherapy alone on survival in glioblastoma in a randomised phase III study: 5-year analysis of the EORTC-NCIC trial, Lancet Oncol. 10 (2009) 459–466.

[4] J. Wang, W. Tang, M. Yang, Y. Yin, H. Li, F. Hu, L. Tang, X. Ma, Y. Zhang, Y. Wang, Inflammatory tumor microenvironment responsive neutrophil exosomes-based drug delivery system for targeted glioma therapy, Biomaterials 273 (2021) 120784.

[5] L. Nieland, L.M. Morsett, M.L.D. Broekman, X.O. Breakefield, E.R. Abels, Extracellular vesicle-mediated bilateral communication between glioblastoma and astrocytes, Trends Neurosci. 44 (2021) 215–226.

[6] A. Becker, B.K. Thakur, J.M. Weiss, H.S. Kim, H. Peinado, D. Lyden, Extracellular vesicles in cancer: cell-to-cell mediators of metastasis, Cancer Cell 30 (2016) 836–848.

[7] Y. Guo, G. Hu, Y. Xia, H. Li, J. Yuan, J. Zhang, Y. Chen, H. Guo, Y. Yang, Y. Wang, Z. Deng, Eliminating the original cargos of glioblastoma cell-derived small extracellular vesicles for efficient drug delivery to glioblastoma with improved biosafety, Bioact. Mater. 16 (2022) 204–217.

[8] O.M. Elsharkasy, J.Z. Nordin, D.W. Hagey, O.G. de Jong, R.M. Schiffelers, S. E. Andaloussi, P. Vader, Extracellular vesicles as drug delivery systems: why and how? Adv. Drug Deliv. Rev. 159 (2020) 332–343.

[9] S. Shan, J. Chen, Y. Sun, Y. Wang, B. Xia, H. Tan, C. Pan, G. Gu, J. Zhong, G. Qing, et al., Functionalized macrophage exosomes with panobinostat and PPM1D-siRNA for diffuse intrinsic pontine gliomas therapy, Adv. Sci. (Weinh.) 9 (2022) e2200353.

[10] L. Rao, L. Wu, Z. Liu, R. Tian, G. Yu, Z. Zhou, K. Yang, H.G. Xiong, A. Zhang, G. T. Yu, et al., Hybrid cellular membrane nanovesicles amplify macrophage immune responses against cancer recurrence and metastasis, Nat. Commun. 11 (2020) 4909.

[11] S.C. Jang, O.Y. Kim, C.M. Yoon, D.S. Choi, T.Y. Roh, J. Park, J. Nilsson, J. Lötvall, Y.K. Kim, Y.S. Gho, Bioinspired exosome-mimetic nanovesicles for targeted delivery of chemotherapeutics to malignant tumors, ACS Nano 7 (2013) 7698–7710.

[12] P. Guo, S. Busatto, J. Huang, G. Morad, M.A. Moses, A facile magnetic extrusion method for preparing endosome-derived vesicles for cancer drug delivery, Adv. Funct. Mater. 31 (2021).

[13] C. Liu, Y. Wang, L. Li, D. He, J. Chi, Q. Li, Y. Wu, Y. Zhao, S. Zhang, L. Wang, et al., Engineered extracellular vesicles and their mimetics for cancer immunotherapy, J. Contr. Release 349 (2022) 679–698.

[14] R.H. Fang, Y. Jiang, J.C. Fang, L. Zhang, Cell membrane-derived nanomaterials for biomedical applications, Biomaterials 128 (2017) 69–83.

[15] J.Y. Wu, Y.J. Li, X.B. Hu, S. Huang, S. Luo, T. Tang, D.X. Xiang, Exosomes and biomimetic nanovesicles-mediated anti-glioblastoma therapy: a head-to-head comparison, J. Contr. Release 336 (2021) 510–521.

[16] R. Qian, K. Wang, Y. Guo, H. Li, Z. Zhu, X. Huang, C. Gong, Y. Gao, R. Guo, B. Yang, et al., Minimizing adverse effects of Cerenkov radiation induced photodynamic therapy with transformable photosensitizer-loaded nanovesicles, J. Nanobiotechnol. 20 (2022) 203.

[17] K. Wang, U.S. Kumar, N. Sadeghipour, T.F. Massoud, R. Paulmurugan, A microfluidics-based scalable approach to generate extracellular vesicles with enhanced therapeutic MicroRNA loading for intranasal delivery to mouse glioblastomas, ACS Nano 15 (2021) 18327–18346.

[18] G. Golinelli, G. Grisendi, M. Dall'Ora, G. Casari, C. Spano, R. Talami, F. Banchelli, M. Prapa, C. Chiavelli, F. Rossignoli, et al., Anti-GD2 CAR MSCs against metastatic Ewing's sarcoma, Transl. Oncol. 15 (2022) 101240.

[19] Y. Zou, Y. Wang, S. Xu, Y. Liu, J. Yin, D.B. Lovejoy, M. Zheng, X.J. Liang, J.B. Park, Y.M. Efremov, et al., Brain Co-delivery of temozolomide and cisplatin for combinatorial glioblastoma chemotherapy, Adv. Mater. 34 (2022) e2203958.

[20] B.M. Andersen, C. Faust Akl, M.A. Wheeler, E.A. Chiocca, D.A. Reardon, F. J. Quintana, Glial and myeloid heterogeneity in the brain tumour microenvironment, Nat. Rev. Cancer 21 (2021) 786–802.

[21] M.D. Sørensen, R.H. Dahlrot, H.B. Boldt, S. Hansen, B.W. Kristensen, Tumour-associated microglia/macrophages predict poor prognosis in high-grade gliomas and correlate with an aggressive tumour subtype, Neuropathol. Appl. Neurobiol. 44 (2018) 185–206.

[22] J. Erbani, M. Boon, L. Akkari, Therapy-induced shaping of the glioblastoma microenvironment: macrophages at play, Semin. Cancer Biol. 86 (2022) 41–56.

[23] A. Okuma, Y. Ishida, T. Kawara, S. Hisada, S. Araki, Secretory co-factors in next-generation cellular therapies for cancer, Front. Immunol. 13 (2022) 907022.

[24] L.A. Stern, S. Gholamin, I. Moraga, X. Yang, S. Saravanakumar, J.R. Cohen, R. Starr, B. Aguilar, V. Salvary, J.C. Hibbard, et al., Engineered IL13 variants direct specificity of IL13Rα2-targeted CAR T cell therapy, Proc. Natl. Acad. Sci. U. S. A. 119 (2022) e2112006119.

[25] L. Lee, B. Draper, N. Chaplin, B. Philip, M. Chin, D. Galas-Filipowicz, S. Onuoha, S. Thomas, V. Baldan, R. Bughda, et al., An APRIL-based chimeric antigen receptor for dual targeting of BCMA and TACI in multiple myeloma, Blood 131 (2018) 746–758.

[26] T. Zhang, B.A. Lemoi, C.L. Sentman, Chimeric NK-receptor-bearing T cells mediate antitumor immunotherapy, Blood 106 (2005) 1544–1551.

[27] C.E. Brown, D. Alizadeh, R. Starr, L. Weng, J.R. Wagner, A. Naranjo, J.R. Ostberg, M.S. Blanchard, J. Kilpatrick, J. Simpson, et al., Regression of glioblastoma after chimeric antigen receptor T-cell therapy, N. Engl. J. Med. 375 (2016) 2561–2569.

[28] K.B. Long, R.M. Young, A.C. Boesteanu, M.M. Davis, J.J. Melenhorst, S.F. Lacey, D. A. DeGaramo, B.L. Levine, J.A. Fraietta, CAR T cell therapy of non-hematopoietic malignancies: detours on the road to clinical success, Front. Immunol. 9 (2018) 2740.
[29] M.M. Boyiadzis, M.V. Dhodapkar, R.J. Brentjens, J.N. Kochenderfer, S.S. Neelapu, M.V. Maus, D.L. Porter, D.G. Maloney, S.A. Grupp, C.L. Mackall, et al., Chimeric antigen receptor (CAR) T therapies for the treatment of hematologic malignancies: clinical perspective and significance, J. Immunother. Cancer 6 (2018) 137.
[30] S.A. Grupp, M. Kalos, D. Barrett, R. Aplenc, D.L. Porter, S.R. Rheingold, D. T. Teachey, A. Chew, B. Hauck, J.F. Wright, et al., Chimeric antigen receptor-modified T cells for acute lymphoid leukemia, N. Engl. J. Med. 368 (2013) 1509–1518.
[31] E. Padfield, H.P. Ellis, K.M. Kurian, Current therapeutic advances targeting EGFR and EGFRvIII in glioblastoma, Front. Oncol. 5 (2015) 5.
[32] S. Ahmad, I. Khan, J. Pandit, N.A. Emad, S. Bano, K.I. Dar, M.M.A. Rizvi, M. D. Ansari, M. Aqil, Y. Sultana, Brain targeted delivery of carmustine using chitosan coated nanoparticles via nasal route for glioblastoma treatment, Int. J. Biol. Macromol. 221 (2022) 435–445.
[33] H. Goel, V. Kalra, S.K. Verma, S.K. Dubey, A.K. Tiwary, Convolutions in the rendition of nose to brain therapeutics from bench to bedside: feats & fallacies, J. Contr. Release 341 (2022) 782–811.
[34] X. Wang, X.L. Lu, H.Y. Zhao, F.C. Zhang, X.B. Jiang, A novel recombinant protein of IP10-EGFRvIIIscFv and CD8(+) cytotoxic T lymphocytes synergistically inhibits the growth of implanted glioma in mice, Cancer Immunol. Immunother. 62 (2013) 1261–1272.
[35] M. Colombo, G. Raposo, C. Théry, Biogenesis, secretion, and intercellular interactions of exosomes and other extracellular vesicles, Annu. Rev. Cell Dev. Biol. 30 (2014) 255–289.
[36] S.D. Ibsen, J. Wright, J.M. Lewis, S. Kim, S.Y. Ko, J. Ong, S. Manouchehri, A. Vyas, J. Akers, C.C. Chen, et al., Rapid isolation and detection of exosomes and associated biomarkers from plasma, ACS Nano 11 (2017) 6641–6651.
[37] Z. Chen, X. Feng, C.J. Herting, V.A. Garcia, K. Nie, W.W. Pong, R. Rasmussen, B. Dwivedi, S. Seby, S.A. Wolf, et al., Cellular and molecular identity of tumor-associated macrophages in glioblastoma, Cancer Res. 77 (2017) 2266–2278.
[38] L. Guo, Y. Zhang, R. Wei, X. Zhang, C. Wang, M. Feng, Proinflammatory macrophage-derived microvesicles exhibit tumor tropism dependent on CCL2/CCR2 signaling axis and promote drug delivery via SNARE-mediated membrane fusion, Theranostics 10 (2020) 6581–6598.
[39] G.O. Ahn, D. Tseng, C.H. Liao, M.J. Dorie, A. Czechowicz, J.M. Brown, Inhibition of Mac-1 (CD11b/CD18) enhances tumor response to radiation by reducing myeloid cell recruitment, Proc. Natl. Acad. Sci. U. S. A. 107 (2010) 8363–8368.
[40] J.M. Mota, C.A. Leite, L.E. Souza, P.H. Melo, D.C. Nascimento, V.M. de-Deus-Wagatsuma, J. Temporal, F. Figueiredo, H. Noushmehr, J.C. Alves-Filho, et al., Post-sepsis state induces tumor-associated macrophage accumulation through CXCR4/CXCL12 and favors tumor progression in mice, Cancer Immunol. Res. 4 (2016) 312–322.
[41] Y.J. Li, J.Y. Wu, J.M. Wang, X.B. Hu, J.X. Cai, D.X. Xiang, Gemcitabine loaded autologous exosomes for effective and safe chemotherapy of pancreatic cancer, Acta Biomater. 101 (2020) 519–530.
[42] L.D. Di Filippo, J.L. Duarte, M.T. Luiz, J.T.C. de Araújo, M. Chorilli, Drug delivery nanosystems in glioblastoma multiforme treatment: current state of the art, Curr. Neuropharmacol. 19 (2021) 787–812.
[43] Q. Xu, Z. Zhang, L. Zhao, Y. Qin, H. Cai, Z. Geng, X. Zhu, W. Zhang, Y. Zhang, J. Tan, et al., Tropism-facilitated delivery of CRISPR/Cas9 system with chimeric antigen receptor-extracellular vesicles against B-cell malignancies, J. Contr. Release 326 (2020) 455–467.
[44] M.J. Pauwels, J. Xie, A. Ceroi, S. Balusu, J. Castelein, E. Van Wonterghem, G. Van Imschoot, A. Ward, T.R. Menheniott, O. Gustafsson, et al., Choroid plexus-derived extracellular vesicles exhibit brain targeting characteristics, Biomaterials 290 (2022) 121830.
[45] Z. Ye, T. Zhang, W. He, H. Jin, C. Liu, Z. Yang, J. Ren, Methotrexate-loaded extracellular vesicles functionalized with therapeutic and targeted peptides for the treatment of glioblastoma multiforme, ACS Appl. Mater. Interfaces 10 (2018) 12341–12350.
[46] S. Peter, S. Alven, R.B. Maseko, B.A. Aderibigbe, Doxorubicin-based hybrid compounds as potential anticancer agents: a review, Molecules (Basel) 27 (2022).
[47] I. Sardi, O. Fantappiè, G. la Marca, M.G. Giovannini, A.L. Iorio, M. da Ros, S. Malvagia, S. Cardellicchio, L. Giunti, M. de Martino, R. Mazzanti, Delivery of doxorubicin across the blood-brain barrier by ondansetron pretreatment: a study in vitro and in vivo, Cancer Lett. 353 (2014) 242–247.
[48] R. Whelan, G.C. Hargaden, A.J.S. Knox, Modulating the blood-brain barrier: a comprehensive review, Pharmaceutics 13 (2021).
[49] T. Lian, R.J. Ho, Trends and developments in liposome drug delivery systems, J. Pharmaceut. Sci. 90 (2001) 667–680.
[50] A. Gabizon, H. Shmeeda, Y. Barenholz, Pharmacokinetics of pegylated liposomal Doxorubicin: review of animal and human studies, Clin. Pharmacokinet. 42 (2003) 419–436.
[51] Y. Barenholz, Doxil®–the first FDA-approved nano-drug: lessons learned, J. Contr. Release : Off.J. Control. Release Soc. 160 (2012) 117–134.
[52] M.R. Islam, J. Patel, P.I. Back, H. Shmeeda, K. Adamsky, H. Yang, C. Alvarez, A. A. Gabizon, N.M. La-Beck, Comparative effects of free doxorubicin, liposome encapsulated doxorubicin and liposome co-encapsulated alendronate and doxorubicin (PLAD) on the tumor immunologic milieu in a mouse fibrosarcoma model, Nanotheranostics 6 (2022) 451–464.
[53] R. Li, X. Zhu, P. Zhou, Y. Qiao, Y. Li, Y. Xu, X. Shi, Generation of a high-affinity nanobody against CD147 for tumor targeting and therapeutic efficacy through conjugating doxorubicin, Front. Immunol. 13 (2022) 852700.
[54] S. Herman, I. Fishel, D. Offen, Intranasal delivery of mesenchymal stem cells-derived extracellular vesicles for the treatment of neurological diseases, Stem Cell. 39 (2021) 1589–1600.
[55] Y. Hu, K. Jiang, D. Wang, S. Yao, L. Lu, H. Wang, J. Song, J. Zhou, X. Fan, Y. Wang, et al., Core-shell lipoplexes inducing active macropinocytosis promote intranasal delivery of c-Myc siRNA for treatment of glioblastoma, Acta Biomater. 138 (2022) 478–490.
[56] K. Chung, I. Ullah, N. Kim, J. Lim, J. Shin, S.C. Lee, S. Jeon, S.H. Kim, P. Kumar, S. K. Lee, Intranasal delivery of cancer-targeting doxorubicin-loaded PLGA nanoparticles arrests glioblastoma growth, J. Drug Target. 28 (2020) 617–626.
[57] Y. Octavia, C.G. Tocchetti, K.L. Gabrielson, S. Janssens, H.J. Crijns, A.L. Moens, Doxorubicin-induced cardiomyopathy: from molecular mechanisms to therapeutic strategies, J. Mol. Cell. Cardiol. 52 (2012) 1213–1225.
[58] K. Renu, G.A. V, B.T. P, S. Arunachalam, Molecular mechanism of doxorubicin-induced cardiomyopathy - an update, Eur. J. Pharmacol. 818 (2018) 241–253.
[59] S.Y. Kim, S.J. Kim, B.J. Kim, S.Y. Rah, S.M. Chung, M.J. Im, U.H. Kim, Doxorubicin-induced reactive oxygen species generation and intracellular Ca2+ increase are reciprocally modulated in rat cardiomyocytes, Exp. Mol. Med. 38 (2006) 535–545.
[60] G.C. Pereira, A.M. Silva, C.V. Diogo, F.S. Carvalho, P. Monteiro, P.J. Oliveira, Drug-induced cardiac mitochondrial toxicity and protection: from doxorubicin to carvedilol, Curr. Pharm. Des. 17 (2011) 2113–2129.
[61] W. Liao, Z. Rao, L. Wu, Y. Chen, C. Li, Cariporide attenuates doxorubicin-induced cardiotoxicity in rats by inhibiting oxidative stress, inflammation and apoptosis partly through regulation of akt/GSK-3β and Sirt1 signaling pathway, Front. Pharmacol. 13 (2022) 850053.
[62] N. Wenningmann, M. Knapp, A. Ande, T.R. Vaidya, S. Ait-Oudhia, Insights into doxorubicin-induced cardiotoxicity: molecular mechanisms, preventive strategies, and early monitoring, Mol. Pharmacol. 96 (2019) 219–232.
[63] Y. Shi, M. Moon, S. Dawood, B. McManus, P.P. Liu, Mechanisms and management of doxorubicin cardiotoxicity, Herz 36 (2011) 296–305.
[64] S. Fogli, P. Nieri, M.C. Breschi, The role of nitric oxide in anthracycline toxicity and prospects for pharmacologic prevention of cardiac damage, FASEB J. 18 (2004) 664–675.
[65] H. Chen, T. Sun, C. Jiang, Extracellular vesicle-based macromolecule delivery systems in cancer immunotherapy, J. Contr. Release 348 (2022) 572–589.
[66] C. Vandendriessche, D. Kapogiannis, R.E. Vandenbroucke, Biomarker and therapeutic potential of peripheral extracellular vesicles in Alzheimer's disease, Adv. Drug Deliv. Rev. 190 (2022) 114486.
[67] X. Wang, S. Hu, J. Li, D. Zhu, Z. Wang, J. Cores, K. Cheng, G. Liu, K. Huang, Extruded mesenchymal stem cell nanovesicles are equally potent to natural extracellular vesicles in cardiac repair, ACS Appl. Mater. Interfaces 13 (2021) 55767–55779.
[68] S. Pisano, I. Pierini, J. Gu, A. Gazze, L.W. Francis, D. Gonzalez, R.S. Conlan, B. Corradetti, Immune (cell) derived exosome mimetics (IDEM) as a treatment for ovarian cancer, Front. Cell Dev. Biol. 8 (2020) 553576.
[69] D. Furtado, M. Björnmalm, S. Ayton, A.I. Bush, K. Kempe, F. Caruso, Overcoming the blood-brain barrier: the role of nanomaterials in treating neurological diseases, Adv. Mater. 30 (2018) e1801362.
[70] G. Batist, G. Ramakrishnan, C.S. Rao, A. Chandrasekharan, J. Gutheil, T. Guthrie, P. Shah, A. Khojasteh, M.K. Nair, K. Hoelzer, K. Tkaczuk, Y.C. Park, L.W. Lee, Reduced cardiotoxicity and preserved antitumor efficacy of liposome-encapsulated doxorubicin and cyclophosphamide compared with conventional doxorubicin and cyclophosphamide in a randomized, multicenter trial of metastatic breast cancer, J. Clin. Oncol. : Off.J. Am. Soc. Clinic. Oncol. 19 (2001) 1444–1454.
[71] C. He, S. Zheng, Y. Luo, B. Wang, E**xosome theranostics: biology and translational medicine**, Theranostics 8 (2018) 237–255.
[72] L. Illum, Nasal drug delivery–possibilities, problems and solutions, J. Contr. Release : Off.J. Control. Release Soc. 87 (2003) 187–198.
[73] Y. Chen, C. Zhang, Y. Huang, Y. Ma, Q. Song, H. Chen, G. Jiang, X. Gao, Intranasal drug delivery: the interaction between nanoparticles and the nose-to-brain pathway, Adv. Drug Deliv. Rev. 207 (2024) 115196.
[74] T.P. Crowe, M.H.W. Greenlee, A.G. Kanthasamy, W.H. Hsu, Mechanism of intranasal drug delivery directly to the brain, Life Sci. 195 (2018) 44–52.
[75] S. Ma, X. Li, X. Wang, L. Cheng, Z. Li, C. Zhang, Z. Ye, Q. Qian, Current progress in CAR-T cell therapy for solid tumors, Int. J. Biol. Sci. 15 (2019) 2548–2560.
[76] J.N. Brudno, J.N. Kochenderfer, Recent advances in CAR T-cell toxicity: mechanisms, manifestations and management, Blood Rev. 34 (2019) 45–55.